Angewandte Chemie
Eine Zeitschrift der Gesellschaft Deutscher Chemiker

Supporting Information

Magneto-Adaptive Surfactants Showing Anti-Curie Behavior and Tunable Surface Tension as Porogens for Mesoporous Particles with 12-Fold Symmetry

*Stefanie Hermann, Martin Wessig, Dennis Kollofrath, Melanie Gerigk, Kay Hagedorn, James A. Odendal, Matthias Hagner, Markus Drechsler, Philipp Erler, Mikhail Fonin, Georg Maret, and Sebastian Polarz**

ange_201612416_sm_miscellaneous_information.pdf

Supporting Information

Experimental Part

Zinc chloride (98%) was purchased from ABCR and used without further purification. 1-Bromodecan (≥ 98%) were purchased from ACROS Organics and used without further purification. Sodium hydrogen carbonate (p.a.) was purchased from Merck Millipore. 1-Bromohexadecane (98%), Tetraethyl orthosilicate (≥ 99% GC grade), manganese (II) chloride tetrahydrate (≥ 98%), nickel (II) chloride hexahydrate (≥ 98%), cobalt (II) chloride hexahydrate (≥ 98%) were purchased from Sigma Aldrich and used without further purification. Acetonitrile (≥ 99.9% HPLC grade) was purchased from Carl Roth, methanol (≥ 99.8% ACS) was purchased from Sigma Aldrich and used without further purification. Ultrapure water was obtained by milli-Q water filtration prior use.

Table S1. Summary of prepared compounds

Number	Description	Molecular Formula	Molecular Mass [g/mol]
(1)	$NiC_{10}DOTA$	$C_{24}H_{44}N_4O_6Ni$	543.33
(2)	$CoC_{10}DOTA$	$C_{24}H_{44}N_4O_6Co$	543.57
(3)	$MnC_{10}DOTA$	$C_{24}H_{44}N_4O_6Mn$	539.58
(4)	$ZnC_{10}DOTA$	$C_{24}H_{44}N_4O_6Zn$	550.02
(5)	$NiC_{16}DOTA$	$C_{30}H_{56}N_4O_6Ni$	627.49
(6)	$CoC_{16}DOTA$	$C_{30}H_{56}N_4O_6Co$	627.73
(7)	$MnC_{16}DOTA$	$C_{30}H_{56}N_4O_6Mn$	623.74
(8)	$ZnC_{16}DOTA$	$C_{30}H_{56}N_4O_6Zn$	634.18
(9)	$C_{10}DOTA$ TFA	$C_{26}H_{47}N_4O_8F_3$	600.68
(10)	$C_{16}DOTA$ TFA	$C_{32}H_{59}N_4O_8F_3$	684.84

Preparation of metal complexes: Ligands C_nDOTA (n = 10, 16) were prepared according to published methods.[1] The introduction of alkyl residues were realized by use of 1-Bromodecane or 1-Bromohexadecane respectively. Complexation of transition metal cation M^{2+} (M = Ni, Co, Mn, Zn) was achieved by stirring C_nDOTA (n = 10, 16) (7.30×10^{-4} mol) with equimolar amount of metal halide (7.30×10^{-4} mol) in methanol (6 mL) for 48 h under reflux following a previously described procedure[1c]. Remaining solid residues were removed by filtration. Excess solvent was removed *in vacuo*. Solid MC_nDOTA (M = Ni^{2+}, Zn^{2+}, Co^{2+}, Mn^{2+}) complexes were quantitatively yielded. For further purification the metal complexes were

recrystallized from water/acetone or water/ethanol and dried in vacuo. The molecular characterization of the prepared surfactants was carried out by electrospray ionization mass spectroscopy (see **figure 1**), elemental analysis and FT-ATR-IR spectroscopy (see figure **S-2b+c**).

Analysis of compounds:

compound (1) sum formula: $C_{24}H_{44}N_4O_6Ni$; ESI-MS [m/z] (exp./theor.) for $[M^-] \equiv [C_{24}H_{43}N_4O_6Ni]^-$: (541.248 / 541.250), (542.256 / 542.260), (543.250 / 543.250), (544.245 / 544.250), (545.241 / 545.250), (546.238 / 546.250), (547.235 / 547.250); FT-ATR-IR $\tilde{\nu}$[cm^{-1}]: 3316, 2925, 2854, 2633, 1731, 1592, 1459, 1432, 1408, 1317, 1292, 1262, 1214, 1156, 1091, 1064, 1063, 1034, 1010, 981, 919, 830, 816, 796, 778, 730, 704.

compound (2) sum formula: $C_{24}H_{44}N_4O_6Co$; ESI-MS [m/z] (exp./theor.) for $[M^-] \equiv [C_{24}H_{43}N_4O_6Co]^-$: (542.274 / 541.250), (543.268 / 543.255), (544.278 / 544.258), (545.262 / 545.274); FT-ATR-IR $\tilde{\nu}$[cm^{-1}]: 2923, 2854, 2633, 1705, 1460, 1417, 1367, 1355, 1326, 1305, 1270, 1244, 1221, 1165, 1121, 1087, 1053, 1009, 990, 981, 969, 930, 911, 831, 804, 789, 749, 721, 692.

compound (3) sum formula: $C_{24}H_{44}N_4O_6Mn$; ESI-MS [m/z] (exp./theor.) for $[M^-] \equiv [C_{24}H_{43}N_4O_6Mn]^-$: (538.259 / 538.262), (539.249 / 539.262), (540.256 / 540.262), (541.263 / 545.262); FT-ATR-IR $\tilde{\nu}$[cm^{-1}]: 3369, 2925, 2854, 2628, 1719, 1594, 1458, 1403, 1358, 1318, 1289, 1238, 1191, 1162, 1086, 1006, 979, 918, 903, 826, 798, 783, 721, 685.

compound (4) sum formula: $C_{24}H_{44}N_4O_6Zn$;

ESI-MS [m/z] (exp./theor.) for $[M^-] \equiv [C_{24}H_{43}N_4O_6Zn]^-$: (547.246 / 547.248), (548.245 / 548.248), (549.244 / 549.248), (550.245 / 550.248), (551.231 / 551.248), (552.248 /552.248), (553.237 /553.248), (554.241 / 554.248); FT-ATR-IR $\tilde{\nu}$[cm^{-1}]: 3369, 2925, 2854, 2628, 1719, 1594, 1458, 1403, 1358, 1318, 1289, 1238, 1191, 1162, 1086, 1006, 979, 918, 903, 826, 798, 783, 721, 685.

compound (5) sum formula: $C_{30}H_{56}N_4O_6Ni$; ESI-MS [m/z] (exp./theor.) for $[M^-] \equiv [C_{30}H_{55}N_4O_6Ni]^-$: (625.345 / 625.347), (626.345 / 626.347), (627.345 / 627.347), (628.345 / 628.347), (629.345 / 629.347), (630.345 / 623.347), (631.345 / 631.347), (632.345 / 632.347); FT-ATR-IR $\tilde{\nu}$[cm^{-1}]: 3278, 2923, 2852, 2613, 1732, 1595, 1464, 1405, 1355, 1314, 1292, 1261, 1213, 1163, 1089, 1066, 1012, 986, 920, 897, 886, 829, 817, 797, 781, 721, 706. elemental analysis calcd (%) for $C_{30}H_{56}N_4O_6Ni$: C 57.42, H 9.00, N 8.93; found: C 57.29, H 9.13, N 8.89.

compound (6) sum formula: $C_{30}H_{56}N_4O_6Co$; ESI-MS [m/z] (exp./theor.) for $[M^-] \equiv [C_{30}H_{55}N_4O_6Co]^-$: (626.344 / 625.347), (627.349 / 626.347), (628.340 / 627.347), (629.360 / 628.347), (629.315 / 629.347); FT-ATR-IR $\tilde{\nu}$[cm^{-1}]: 3337, 2924, 2852, 2622, 1735, 1652, 1462, 1431, 1392, 1357, 1311, 1274, 1247, 1221, 1203, 1168, 1085, 1060, 1015, 1004, 979, 926, 908, 893, 836, 800, 787, 722, 701, 676. elemental analysis calcd (%) for $C_{30}H_{56}N_4O_6Co$: C 57.40, H 8.99, N 8.93; found: C 55.50, H 8.86, N 8.88.

compound (7) sum formula: $C_{30}H_{56}N_4O_6Mn$; ESI-MS [m/z] (exp./theor.) for $[M^-] \equiv [C_{30}H_{55}N_4O_6Mn]^-$: (622.341 / 622.347), (623.342 / 623.347), (624.344 / 624.347), (625.347 / 625.347), (626.355 / 626.347); FT-ATR-IR $\tilde{\nu}$[cm^{-1}]: 3353, 2923, 2853, 2610, 1732, 1683, 1593, 1461, 1406, 1389, 1364, 1316, 1290, 1205, 1192, 1089, 1016, 937, 920, 905, 827, 797, 782, 721, 681. elemental analysis calcd (%) for $C_{30}H_{56}N_4O_6Mn$: C 57.77, H 9.05, N 8.98; found: C 54.25, H 8.27, N 8.48.

compound (8) sum formula: $C_{30}H_{56}N_4O_6Zn$; ^{1}H NMR (400MHz, [D$_6$]DMSO, 25°C, TMS): δ = 0.85 (t, 3H, CH_3 alkyl), 1.24 (m, 26H, CH_2 alkyl), 1.28 (m, 2H, CH_2), 1.47 (m,), 1.62 (m,), 2.70 – 4.40 (m, 24H, CH_2 DOTA cyclene, CH_2, C*H*$_2$C(O)O DOTA CH_2 alkyl), 12.8 (s, 1H, COO*H* cyclene); ESI-MS [m/z] (exp./theor.) for $[M^-]\equiv[C_{30}H_{55}N_4O_6Zn]^-$: (633.335 / 633.341), (634.335 / 634.341), (635.335 / 635.341), (636.347 / 636.341), (637.355 / 637.341), (638.355 / 638.341); FT-ATR-IR $\tilde{\nu}$[cm^{-1}]: 3353, 2923, 2853, 2610, 1732, 1683, 1593, 1461, 1406, 1389, 1364, 1316, 1290, 1205, 1192, 1089, 1016, 937, 920, 905, 827, 797, 782, 721, 681. elemental analysis calcd (%) for $C_{30}H_{56}N_4O_6Zn$: C 56.91, H 8.76, N 8.85; found: C 52.99, H 8.54, N 8.30.

compound (9) sum formula: $C_{26}H_{47}N_4O_8F_3$; ^{1}H NMR (400MHz, [D$_6$]DMSO, 25°C, TMS): δ = 0.86 (t, 3H, CH_3 alkyl), 1.26 (m, 28H, CH_2 alkyl), 2.08 (s, 6H, CH_2), 2.73 - 4.20 (m, 16H, CH_2, cyclene DOTA), 8.05 (s, 1H, NH), 12.3 (s, 3H, C(O)OH); ^{13}C NMR (100.6 MHz, [D6]DMSO, 25°C, TMS): δ = 172.6 (3C, C(O)OH DOTA), 157.9 (1C q, F_3CCOOH TFA), 117.3 (1C q, F_3CCOOH TFA), 46.9 – 54.0 (12C, CH_2 cyclene DOTA), 31.27 (1C, CH_2 alkyl), 28.93 (3C, CH_2 alkyl), 28.89 (1C, CH_2 alkyl), 28.68 (1C, CH_2 alkyl), 26.03 (1C, CH_2 alkyl), 22.08 (1C, CH_2 alkyl), 13.94 (1C, CH_3 alkyl) ESI-MS [m/z] (exp./theor.) for $[MH^+]\equiv[C_{24}H_{46}N_4O_6]^+$: (487.327 / 487.350), (488.337 / 488.350), (489.348 / 489.350), (490.346 / 490.350) $[MNa^+]\equiv[C_{24}H_{45}N_4O_6Na]^+$: (509.312 / 509.350), (510.315 / 509.350), (511.315 / 509.350), (512.315 / 509.350); FT-ATR-IR $\tilde{\nu}$[cm^{-1}]: 3353, 2923, 2853, 2610, 1732, 1683, 1593, 1461, 1406, 1389, 1364, 1316, 1290, 1205, 1192, 1089, 1016, 937, 920, 905, 827, 797, 782, 721, 681.

compound (10) sum formula: $C_{32}H_{59}N_4O_8F_3$; ^{1}H NMR (400MHz, [D$_6$]DMSO, 25°C, TMS): δ = 0.85 (t, 3H; CH_3 alkyl), 1.24 (m, 24H; CH_2 alkyl), 1.28 (m, 2H; CH_2 alkyl), 1.61 (m, 2H; CH_2 alkyl), 2.87 – 3.88 (m, 24H; CH_2 cyclene, CH_2 C*H*$_2$C(O)O), 12.2 (s, 4H, C(O)O*H* DOTA, COO*H* TFA) ; ^{13}C NMR (100.6 MHz, [D6]DMSO, 25°C, TMS): δ = 172.7 (3C, *C(*O)OH DOTA), 158.0 (1C q, F_3CCOOH TFA), 117.2 (1C q, F_3CCOOH TFA), 54.1 (2C, CH_2 DOTA cyclene), 53.4 (1C, CH_2 alkyl), 52.6 (2C, CH_2 DOTA cyclene), 51.8 (2C, CH_2 DOTA cyclene), 50.0 (2C, CH_2 DOTA cyclene), 48.2 (2C, CH_2 DOTA cyclene), 47.3 (2C, CH_2 DOTA cyclene), 31.3 (1C, CH_2 alkyl), 29.03 (8C, CH_2 alkyl), 28.98 (1C, CH_2 alkyl), 28.67 (1C, CH_2 alkyl), 26.0 (1C, CH_2 alkyl), 22.06 (1C, CH_2 alkyl), 13.9 (1C, CH_3 alkyl) ^{19}F NMR (376MHz, [D$_6$]DMSO, 25°C, TMS): δ = - 73.5 (3F;C*F*$_3$ TFA) ESI-MS [m/z] (exp./theor.) for $[MH^+]\equiv[C_{30}H_{58}N_4O_6]^+$: (571.412 / 571.436), (572.412 / 572.436), (573.412 / 573.436), (574.412 / 574.436) $[MNa^+]\equiv[C_{24}H_{45}N_4O_6Na]^+$: (593.402 / 593.420), (594.402 / 594.420), (595.402 / 595.420), (596.402 / 596.420); FT-ATR-IR $\tilde{\nu}$[cm^{-1}]: 3404, 3086, 2924, 2854, 2540, 1722, 1662, 1464, 1400, 1386, 1353, 1317, 1301, 1182, 1132, 1086, 1032, 988, 970, 923, 905, 881, 824, 798, 784, 718, 677.

Formation of emulsions: Surfactants MC_nDOTA were dissolved in water (miliQ-standard) resulting in clear solutions (c = 32 mM). Sodium hydroxide was added (1 : 10^{-4} n/n) and ethyl acetate was added to the clear solution (15 : 1 v/v). Micro emulsions were prepared by ultrasonication treatment within 300 sec. followed by shaking for a duration of 120 sec resulting in clear solutions. The resulting micro emulsions were analysed by dynamic light scattering.

Preparation of $MC_{16}DOTA@SiO_2$ particles via sol-gel synthesis: 1 mL of the as prepared emulsions was magnetically stirred at 800 rpm using a magnetic stirrer (B < 1 T) and tetraethylorthosilicat (TEOS) (26 µL; 0.12 mmol) was quickly added at 298 K. The gained sol was hydrolysed until a clear solution was obtained. Once the solution is clear, the prepared sol was aged for 3 d without magnetically stirring at 298 K. Colourless solid precipitates were

formed and washed by several centrifugation steps with ultrapure water at 298 K. The yielded colourless $C_{16}M@SiO_2$ particles were dried at 313 K for 2 d followed by drying *in vacuo*. Calcination of the prepared silica-materials was conducted at 773 K for 10 h.

During the sol-gel synthesis in order to gain the silica particles the aqueous solution containing surfactant oil in water emulsion droplets was magnetically stirred during the TEOS (Tetraethylorthosilicate) precursor was hydrolysed and further condensation takes place. The prepared gel was aged to gain the resulting silica particles without stirring and without external applied magnetic fields. A suitable idea is deciding the condensation step (when the micelles associated with hydrolysed TEOS precursor (synergistic co-assembly, SCO) are interconnecting) as the step where a magnetic field would have the strongest influence so we decided to build up the experimental setup like mentioned.

Analytical procedures.

ESI-MS data were acquired on a Bruker Microtof II system. The analyses were conducted by direct injection of solutions of the shown samples in water/acetronitrile (1:1 v:v) in the evaporation chamber. ^{1}H-NMR (400 MHz) spectra were measured on a Bruker Avance III operating at 298 K in D_2O. ATR-FT-IR spectra of solid dry samples were performed on a Perkin Elmer Spectrum 100 device. SQUID measurements were conducted on a MPMS XL SQUID magnetometer (Quantum Design) at 1.8 K. Surface tension measurements were performed on a Krüss K1 machine. Sessile drop analysis of aqueous solutions of **7** and **8** (c > cmc, equimolar concentration) were realized by placing a drop (V = 20 µL) on a cleaned and dried polystyrene surface at 298 K. The shape of the droplets were immediately monitored by photographs in absence and presence of a weak magnetic field (B < 1 T in close proximity at approximately 3 mm using a commercially available permanent NdFeB magnet). Pending drop experiments were conducted by forming a small droplet of aqueous solutions (c > cmc, equimolar concentration) of **7** and **8** at the tip of identical PTFE tubes at 298 K. The deformation of the droplets in presence and absence of a weak magnetic field (B < 1 T using a commercially available permanent NdFeB magnet) was immediately monitored by photographs. Dynamic light scattering measurements of aqueous samples of surfactants and emulsions were measured on a Perkin Elmer 100 device. TEM analyses were performed on Zeiss Libra 120 and JEOL JEM-2200 FS machines. The dry solid samples were placed on a carbon coated copper-grid (Mesh 400). For *cryo*-TEM freshly prepared and filtered (pore size 450nm) aqueous micellar solutions (c = 20 mM) of the surfactants were spread on carbon coated Cu-grids. The resulting thin film was virtrified by quickly plunging the grid in liquid ethane at its freezing point. SAXS was performed on a Bruker Nanostar device equipped with a pinhole collimator on a CuK_a radiation source. EPR spectra were recorded on a table-top X-band spectrometer MiniScope MS 400 (Magnet-Tech) equipped with a temperature controller H03 (Magnet-Tech). SEM was conducted on a Zeiss Crossbeam 1540 XB system equipped with EDX. Focused ion beam (FIB) lamella cut was performed using a high performance FIB column equipped with a Ga-Ion beam gun. N_2-Physisorption measurements of solid dry porous samples were performed on a Tristar (Micromeritics) device.

The crystal structure was solved by direct methods (SHELXS-97[2]), completed by difference Fourier syntheses and refined according to the full-matrix-least-square method (SHELXL-97). The program X-Seed[3] was used as an interface to the SHELX programs. The molecular structure plot and packing diagram were prepared with Diamond 4.2.0 (crystal Impact GbR). The crystal data are available at Cambridge Crystallographic Data Center assigned to deposition number CCDC 1450242. Crystal data for NiC_{10}DOTA: $C_{24}H_{46}N_4NiO_{7.12}$, Mr = 563.30 g mol^{-1}, 0.31 x 0.03 x 0.01 mm, colourless needle, triclinic space group P -1 (No. 0), a = 6.9777(8) Å, b = 19.261(2) Å, c = 20.705(3) Å, α = 95.481(11) °, β = 99.109(10) °, γ = 90.075(9) °, V = 2734.7(6) Å^3, Z = 4, $\rho_{calc.}$ = 1.368 g cm^{-3}, µ = 0.758 mm^{-1}, F(000) = 2432,

Mo K_α (λ = 0.71073 Å), T = 100 K, θ_{min} = 1.53 °, θ_{max} = 26.83 °, reflections collected / unique = 37290 / 11438, R_{int} = 0.0627, completeness to θ = 99,7 %, absorption correction: integration, T_{min} = 0.798, T_{max} = 0.991, data / restraints / parameters = 1143 / 44 / 682, goodness-of-fit on F^2 = 1.064, final R indices [$I > 2\sigma(I)$]: R_1 = 0.0671, wR_2 = 0.1488, all data: R_1 = 0.0963, wR_2 = 0.1620, largest diff. peak and hole = 0.593 and – 0.855. Data were collected by using a STOE IPDS II diffractometer equipped with a graphite monochromated Mo-radiation source and the reflections were detected by an image detector plate system.

Magnetoptical effects were measured using the following setup:

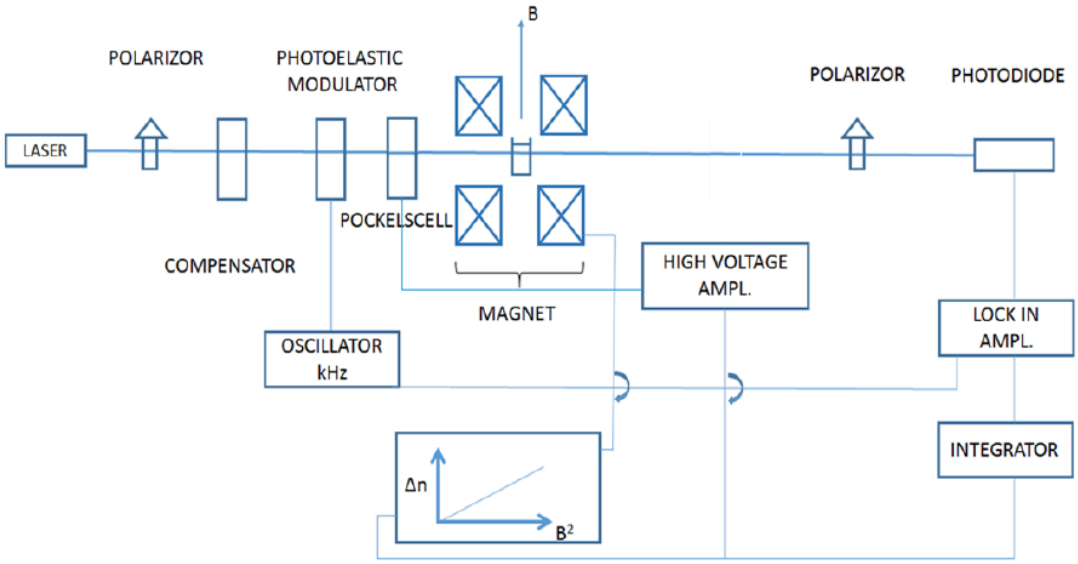

We used magnetic field-induced optical birefringence (*Δn)* with a superconductive solenoid magnet producing a homogeneous magnetic field with a capability of producing 7 T (Tesla) perpendicular to our sample, a laser (HeNe, 633.2 nm) was used, with a continuous compensating feedback modulation technique.[4] The *Δn* were recorded at constant temperature T (± 0.01 °C) during a slow up and down sweeps of the magnetic field *B* at a rate of 0.0038 T/s.

SI-1. Crystallographic data for $NiC_{10}DOTA$

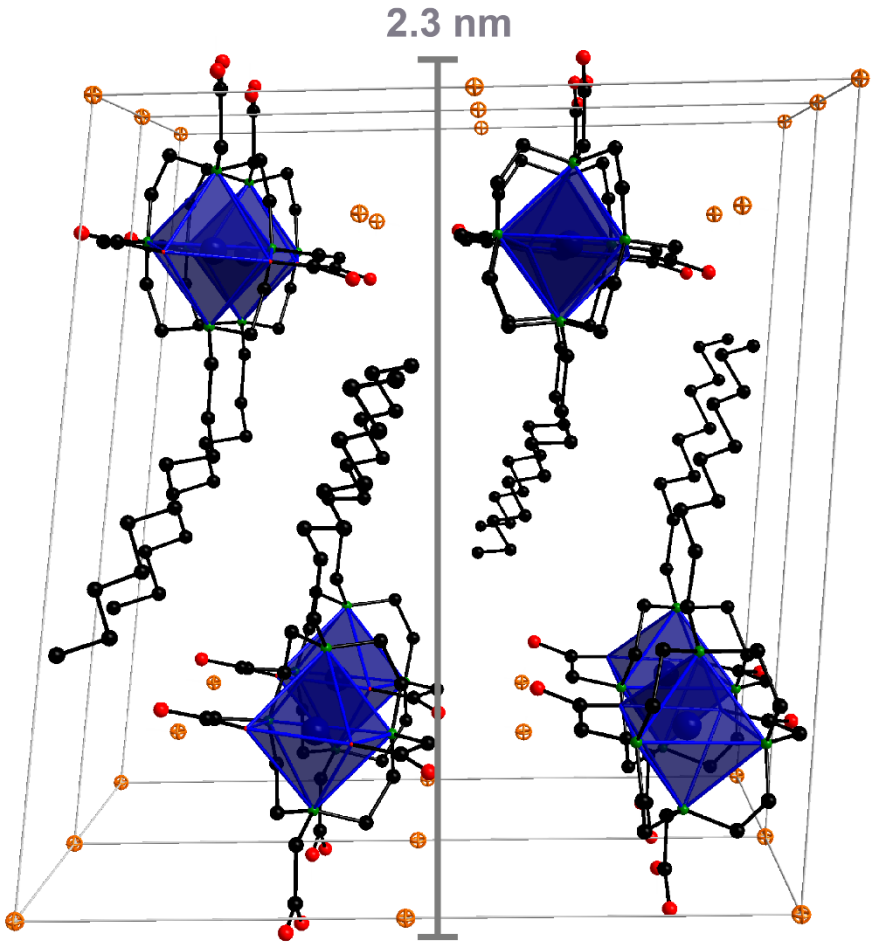

Lamellar crystal packing of $NiC_{10}DOTA$ showing partially interdigitating alkyl chains. (C: black; N: green; O: red; O (water): orange; Ni: blue; H-atoms are ommitted for clarity; unit cell edges: grey line). The lamella distance (head-to-head) is indicated by the grey bold line.

The solid-state packing arrangement of $NiC_{10}DOTA$ shows that this surfactant system self-assembles into a lamellar structure. The hydrophilic head group of this surfactant is packed in a head-to-head manner; this is bridged by a hydrogen bonding interaction of water molecules and the protonated carboxylic acid groups of the head groups. This lamellar packing arrangement is further stabilized by the hydrophobic tails alkyl-alkyl interaction with one another. The crystallographic modelling of the alkyl chains shows some disorder of the carbon atoms. The water molecules and alkyl chains were modelled with some disorder. This is a common phenomenon in crystal structures bearing long alkyl chains and water a consequence of thermal motion in the solid-state.[5] The crystal structure shows that the Ni cation has an octahedral coordination geometry due to its interaction with four nitrogen atoms and two oxygen atoms from the DOTA ligand resulting in an M^{2+} transition metal cation. This coordination motif of DOTA is known for M^{2+} transition metal cations.[6] A table containing a selection of the distance and angle of the octahedral coordination of the Ni cation to the DOTA head group is given below. The distance between of the surfactant lamellar structure is 2.3 nm (see grey line indicating the lamella distance).

Table S2. Selected geometric parameters (Å, °) for $NiC_{10}DOTA$.

Ni_1—N_{22}	2.167 (4)	Ni_1—O_3	2.019 (2)
Ni_1—N_{12}	2.132 (3)	Ni_1—O_{1A}	2.015 (6)
Ni_1—N_{30}	2.181 (5)	Ni_1—O_{1B}	2.16 (2)
Ni_1—N_6	2.127 (3)		
Ni_2—N_8	2.132 (3)	Ni_2—O_4	2.019 (3)
Ni_2—N_{24}	2.171 (5)	Ni_2—O_{2A}	2.17 (2)
Ni_2—N_{11}	2.136 (3)	Ni_2—O_{2B}	2.062 (5)
Ni_2—N_{22}	2.170 (5)		

O_{1A}—Ni_1—O_3 87.56 (18)	O_{1A}—Ni_1—N_6 170.14 (19)
O_3—Ni_1—N_6 82.66 (11)	O_{1A}—Ni_1—N_{12} 82.59 (18)
O_3—Ni_1—N_{12} 170.09 (11)	N_6—Ni_1—N_{12} 107.17 (11)
O_{1A}—Ni_1—O_{1B} 14.9 (6)	O_3—Ni_1—O_{1B} 89.0 (6)
N_6—Ni_1—O_{1B} 164.1 (6)	N_{12}—Ni_1—O_{1B} 81.7 (6)
O_{1A}—Ni_1—N_{23} 99.3 (2)	O_3—Ni_1—N_{23} 98.98 (13)
N_6—Ni_1—N_{23} 83.54 (14)	N_{12}—Ni_1—N_{23} 83.74 (14)
O_{1B}—Ni_1—N_{23} 84.4 (6)	O_{1A}—Ni_1—N_{30} 96.7 (2)
O_3—Ni_1—N_{30} 96.19 (14)	N_6—Ni_1—N_{30} 83.20 (15)
N_{12}—Ni_1—N_{30} 83.94 (15)	O_{1B}—Ni_1—N_{30} 111.3 (6)
N_{23}—Ni_1—N_{30} 158.37 (12)	

SI-2. Additional analytical data for the molecular characterization of the MC_nDOTA surfactants.

(a) $ZnC_{16}DOTA$ ^{1}H-NMR spectroscopy.

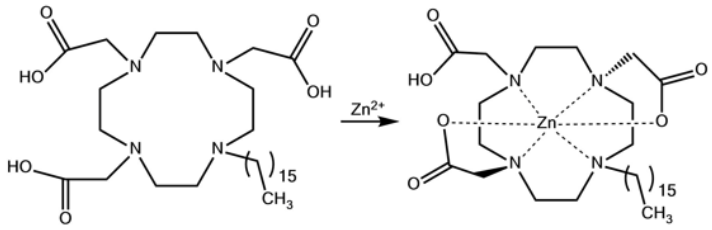

Comparison of $C_{16}DOTA$ (grey) and $ZnC_{16}DOTA$ (black)

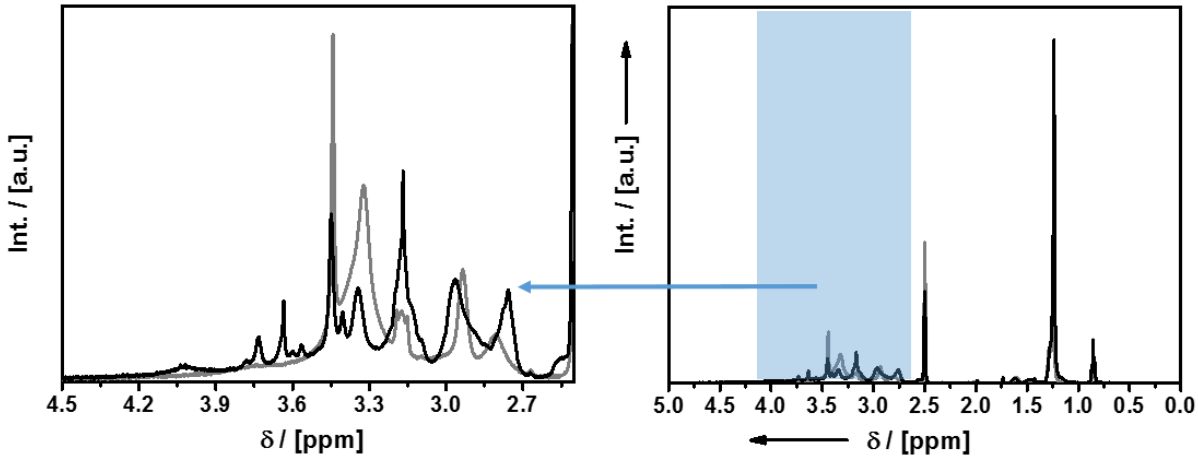

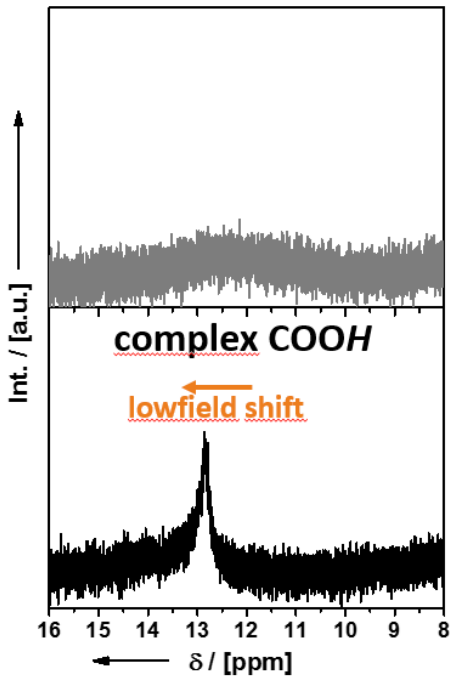

Complexation of Zn^{2+} cation leads to changes in headgroup protons CH_2-region (cyclene ring). (Lowfield shift by withdrawing of electron density).

(b) FT-IR spectroscopy (COO-region).

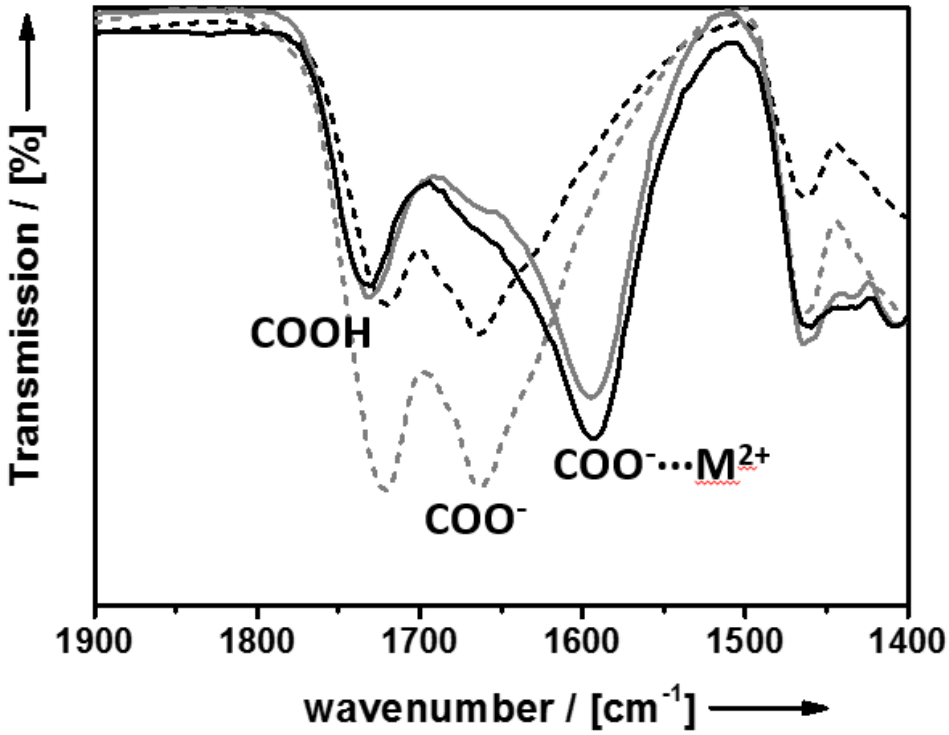

C_{10}DOTA (black, dashed line), C_{16}DOTA (grey, dashed line), NiC_{10}DOTA (black, solid line) and NiC_{16}DOTA (grey, solid line). It can be seen that the chain length does not influence the coordination of Ni^{2+}. Thus, it can be assumed that also for NiC_{16}DOTA occupies the central position in the head group as for NiC_{10}DOTA clarified by single crystal analysis (see Fig. 1 in the main manuscript part).

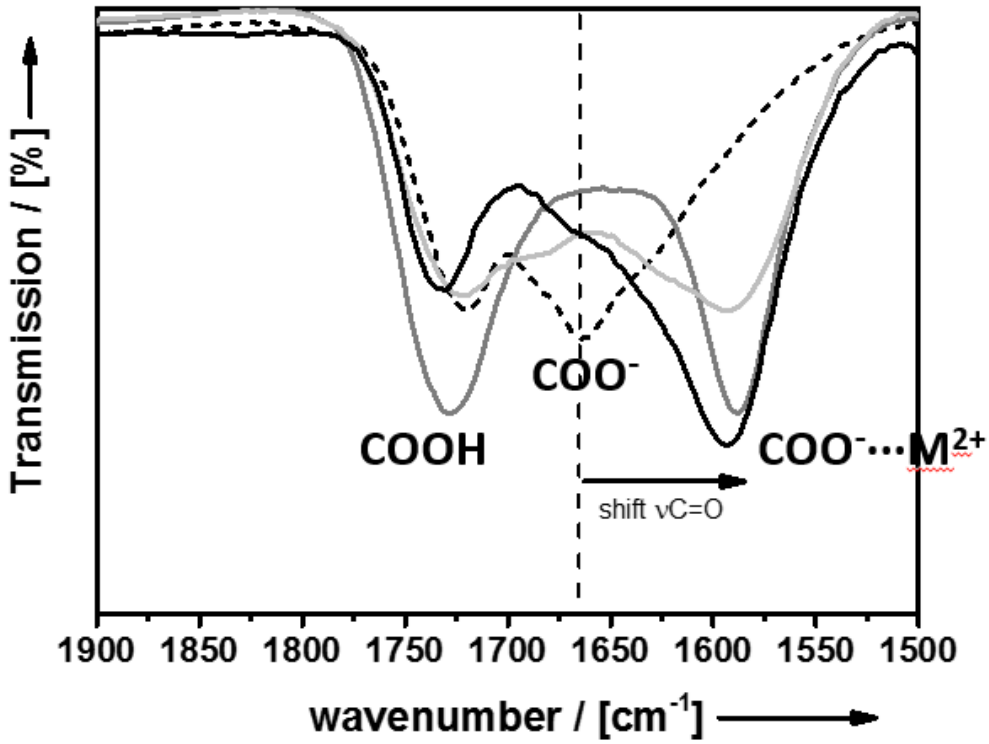

C_{10}DOTA (black dashed), NiC_{10}DOTA (black), ZnC_{10}DOTA (grey) and MnC_{10}DOTA (light). There are only minor differences for the different cations coordinating to the DOTA head. Therefore, it can be concluded that all cations coordinate as proposed in scheme 1 (main manuscript part).

SI-3. Magnetic analysis of solid samples of paramagnetic $MC_{16}DOTA$ compounds.

(a) SQUID

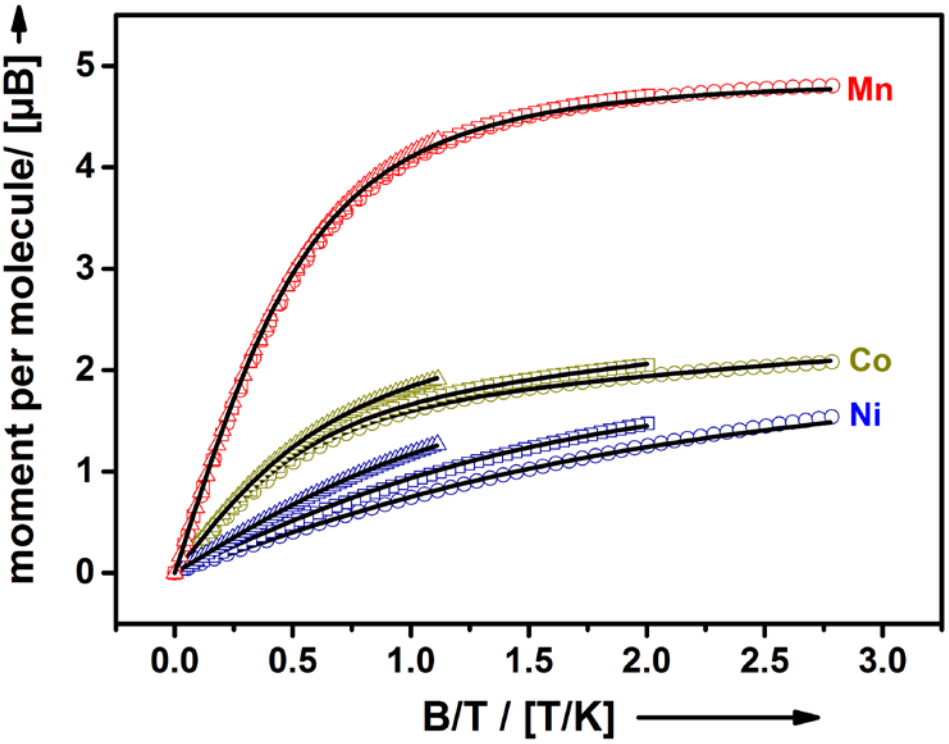

Isothermal magnetization curves of polycrystalline powder samples of $MC_{16}DOTA$ as obtained by SQUID magnetometry at T = 1.8 K (circles), 2.5 K (squares) and 4.5 K (triangles) for M = Ni (blue markers, sample mass ms = 3.6 mg), M = Co (yellow markers, ms = 14.1 mg) and M = Mn (red markers, ms = 7.6 mg). Solid black lines are fits to the data using the following model: For M = Mn, the fit is based on the assumption of a magnetic moment per molecule of $g\mu_B J B_J(\frac{g\mu_B JB}{k_B T})$, where g is the g-factor, J = 5/2 is the total spin quantum number and $B_J(x)$ is the Brillouin function. For M = Ni and M = Co, the fits were performed by diagonalizing spin Hamiltonian $\hat{\mathcal{H}} = D\hat{S}_z^2 + g\mu_B \hat{\boldsymbol{S}} \cdot \boldsymbol{B}$ that contains an axial zero-field splitting (ZFS) and Zeeman term. Here, D is the axial ZFS parameter, $\hat{\boldsymbol{S}}$ is the spin operator and $\hat{S}_z$ is the component of $\hat{\boldsymbol{S}}$ in direction of the magnetic anisotropy axis. The spin quantum number was set to S = 2/2 and S = 3/2 for M = Ni and M = Co, respectively. The obtained best-fit parameters are g = 1.93±0.03 for M = Mn, g = 1.92±0.05, D = (4.92±0.09) cm^{-1} for M = Ni and g = 2.24±0.02, D = −(11.9±0.2) cm^{-1} for M = Co.

(b) EPR of $MnC_{16}DOTA$

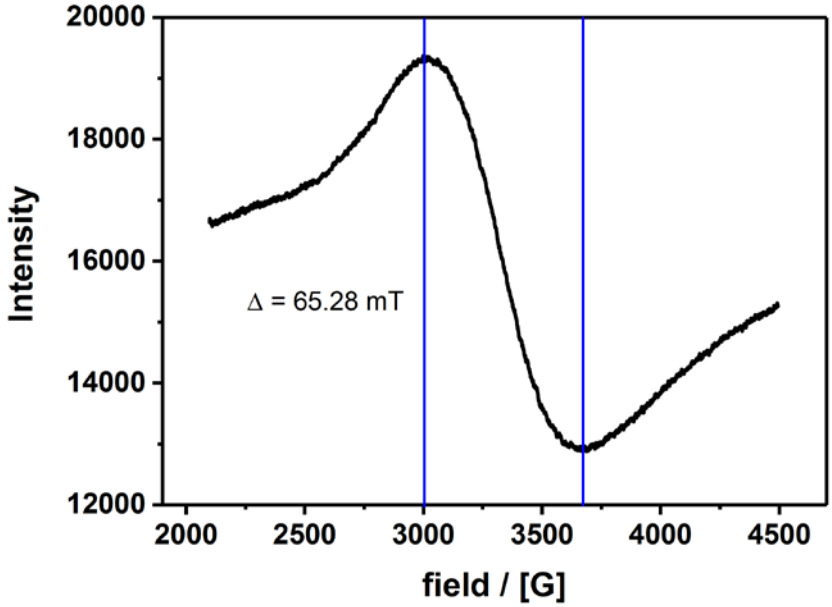

The dipolar coupling between the head groups in the solid-state is so strong that the six lines cannot be seen anymore, and instead only one signal remains.

SI-4. Initial tests regarding surfactant behavior of the MC_nDOTA compounds.

(a) Foaming tests

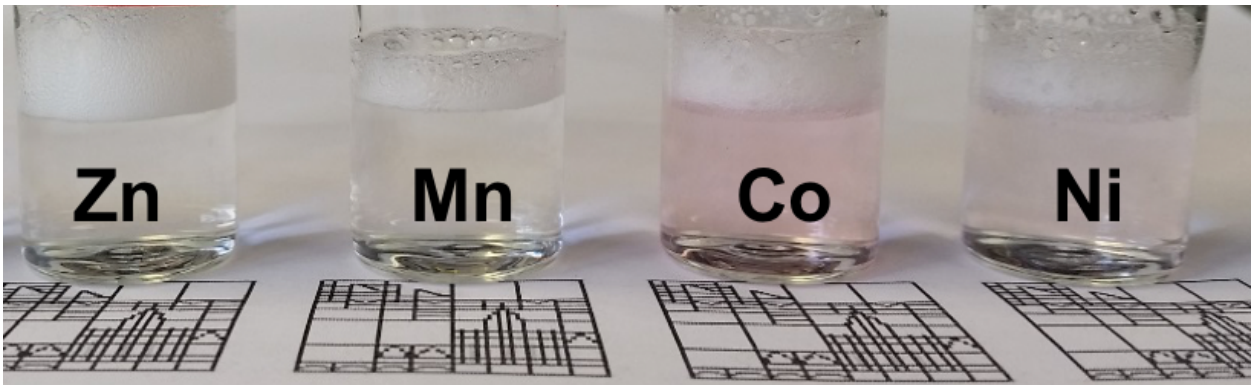

(b) Emulsification tests (water/ ethylacetate (EE) or water/ chloroform (CL).

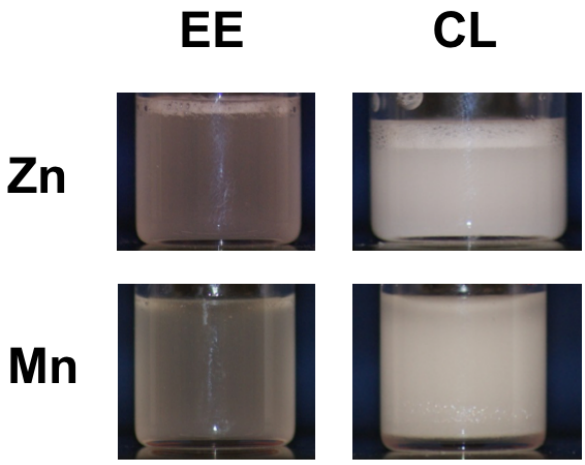

H_2O (15v) : oil (1v)
(EE = ethylacetate; CL = chloroform)

(c) Stability of emulsions checked by DLS.

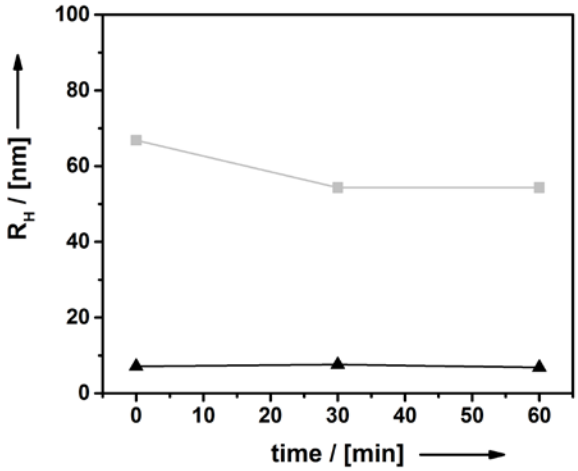

Black data: ethylacetate/water emulsion (15:1 v:v), grey data: chloroform/water emulsion (15:1 v:v).

(d) TEM micrograph of an emulsion water/EE stabilized by $MnC_{16}DOTA$.

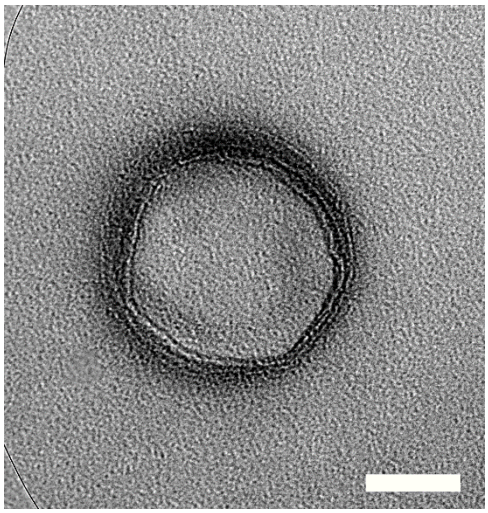

scalebar = 50nm

SI-5. Surface tension measurements of metal containing surfactants.

(a) Paramagnetic surfactant (Mn).

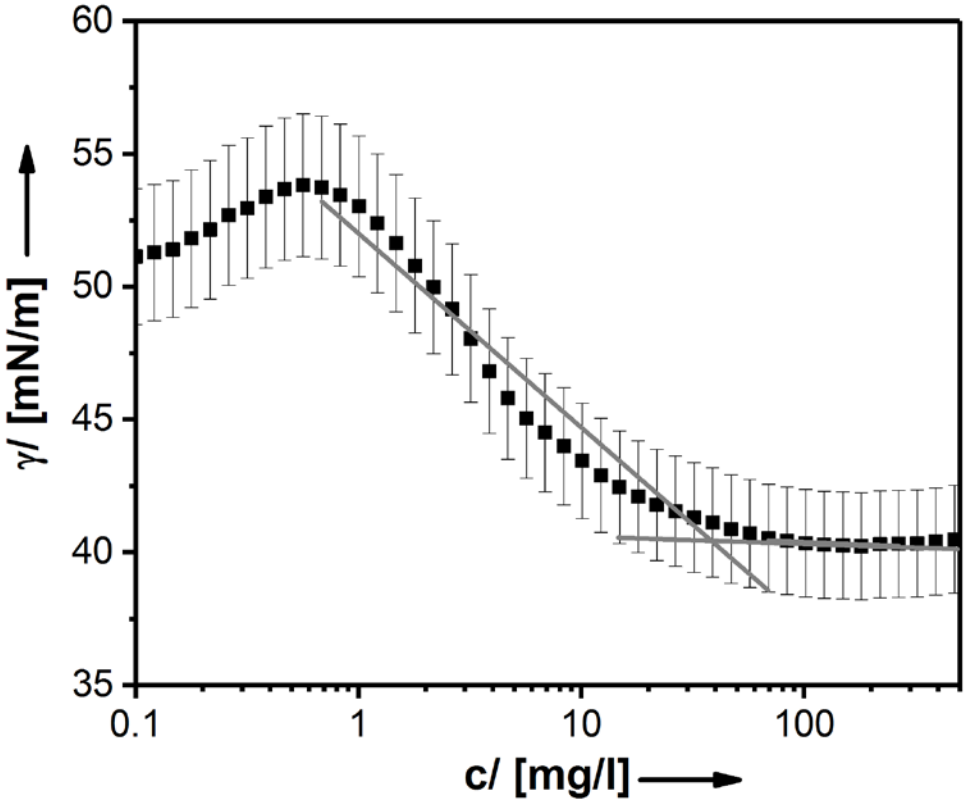

(b) Diamagnetic surfactant (Zn).

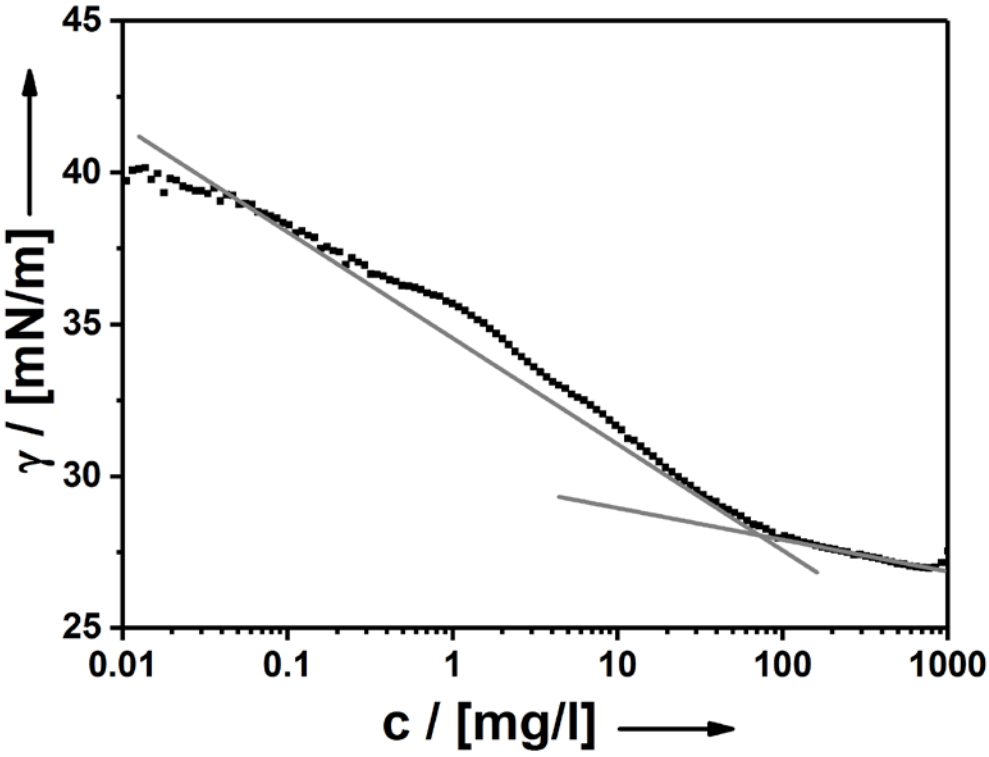

SI-6. DLS data.

(a) Representative particle size distribution function.

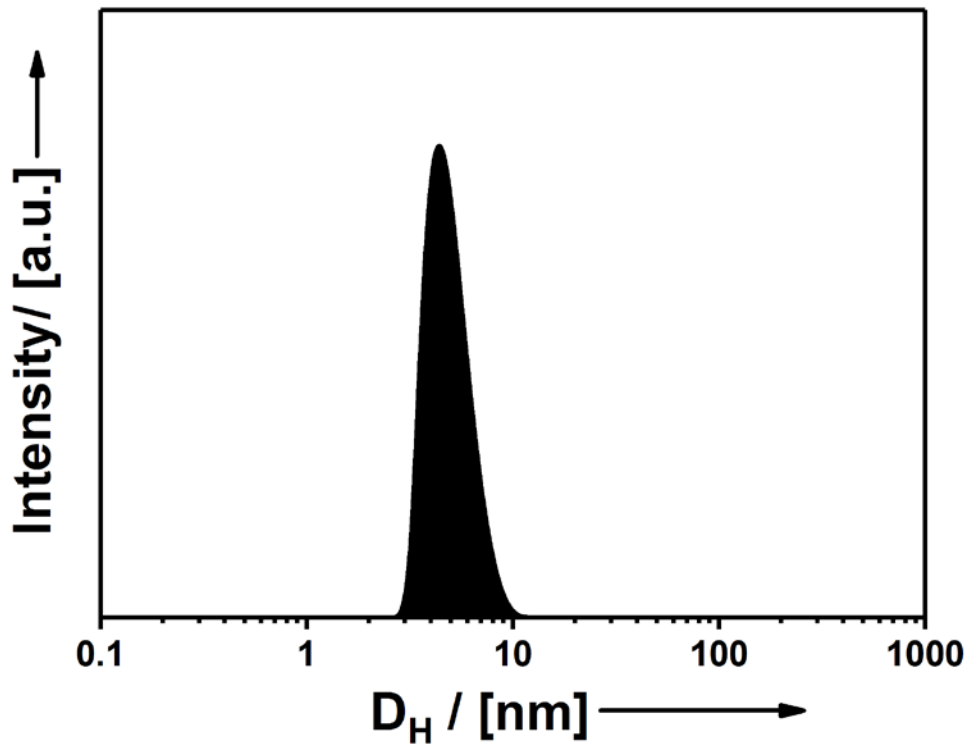

The DLS data show that there is only one aggregate species in solution.

(b) Autocorrelation function of a micellar dispersion of $MnC_{16}DOTA$ in water.

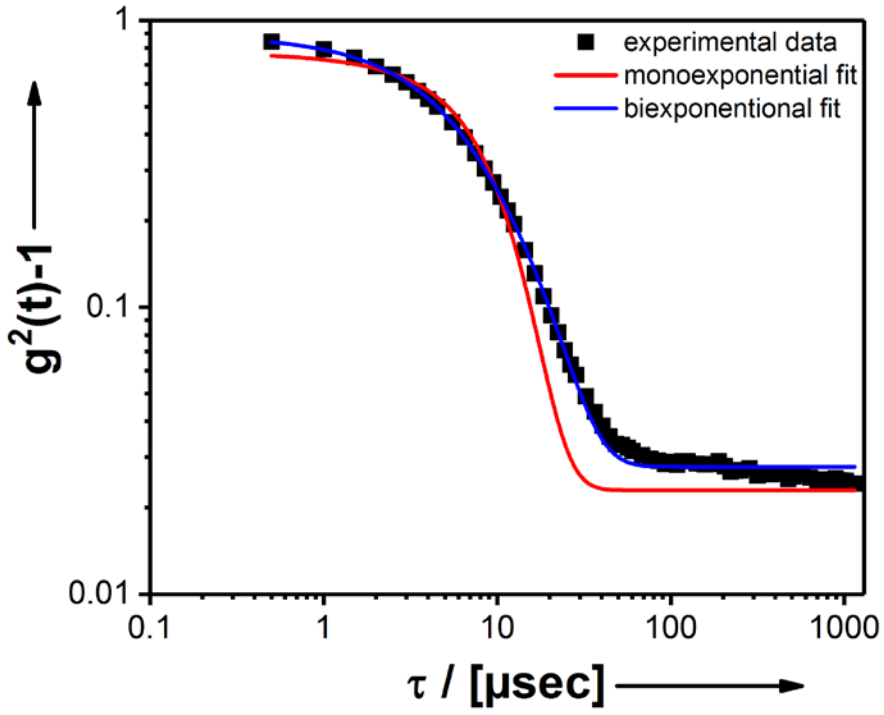

As described by others [7] a deviation from the mono-exponential decay in the autocorrelation function can be assigned to a particle anisotropy.

(c) Geometrical considerations on self-aggregated structures of MC16DOTA (M: Zn, Mn).

Taking in account the classical packing parameter of the surfactants we have described in the manuscript as one of the structure determining parameters which is described by the following equation: $p = \frac{V}{a_0 * l_c}$. Where the packing parameter (p) is determined by the Volume of the surfactant molecule (V), the surface area of the polar head group (a_0) and the critical length of the hydrophobic chain (l_c). Obviously the surface area of the polar headgroup should only be effected by the metal cation complexed by the surfactant. As the mentioned cations are complexed in the same fashion (octahedral, coordination number six) as we have shown in the main manuscript by single crystal x-ray analysis of a Ni^{2+} derivative (**figure 1**) in combination with ATR-infrared spectroscopy and also superconducting quantum interference device (SQUID) magnetometry analyses we now focus on the cation radii and their influences on the effective head group area. The effective head group area of $ZnC_{16}DOTA$ was determined as a_0 = 0.498 nm^2 and for $MnC_{16}DOTA$ the head group area was determined as a_0 = 0.493 nm^2 by force field optimized molecular structures based on the molecular structure of the Ni^{2+} derivative. Force field optimized calculations of the surfactants reveal a packing parameter for $MnC_{16}DOTA$ p = 0.303 and for $ZnC_{16}DOTA$ p = 0.295 which both fulfil the requirements for p < 1/3 which should in both cases result in spherical micelles. Rod-like micelles would be expected with packing parameters of 1/3 < p < 1/2.

Fig. SI-7. Contact angle measurements on sessile drops containing deliberately added Mn^{2+} ions

(a) $ZnC_{16}DOTA+ Mn^{2+}$

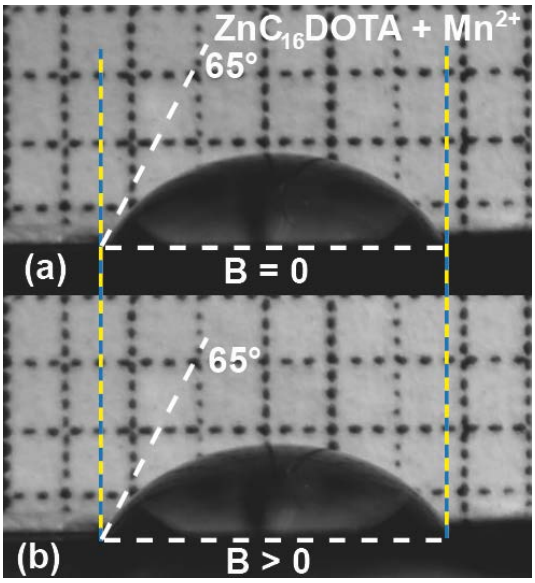

(b) $H_2O + Mn^{2+}$

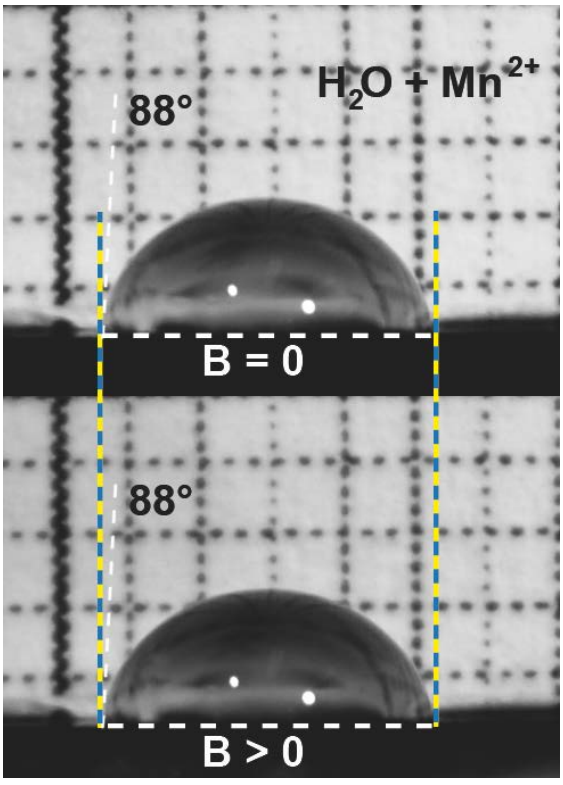

Neither the addition of paramagnetic ions Mn^{2+} to a diamagnetic solution of $ZnC_{16}DOTA$ surfactant (SI-7a) nor the addition of Mn^{2+} salt to pure water (SI-7b) turns the droplets into magnetoresponsive surfaces. Herein it can be concluded that the effects observed in **figure 3b-e** (main manuscript part) are arising because the paramagnetic ion is incorporated in the surfactants head group. The concentration of Mn2+ ions was maintained equal to the experiment shown in **figure 3 b-e**.

Fig. S-8. Mesoporous materials prepared using the diamagnetic ZnC_{16}DOTA as a structure-directing agent.

(a) SEM micrograph of mesoporous particles.

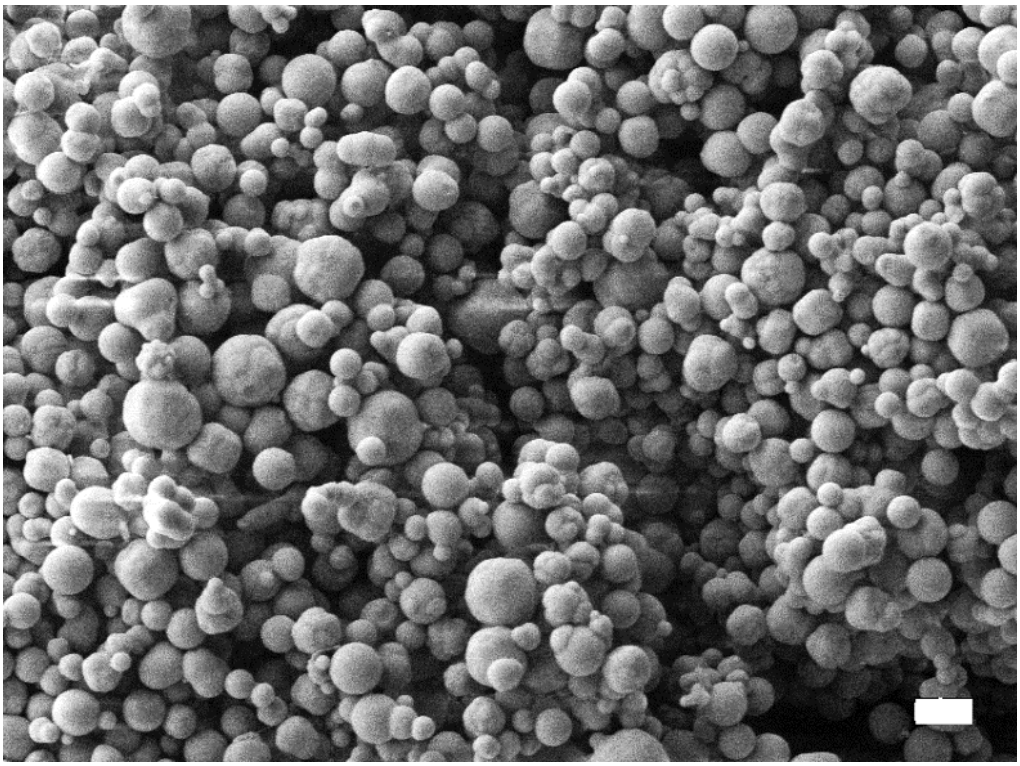

scalebar = 1 μm

(b) SAXS analysis.

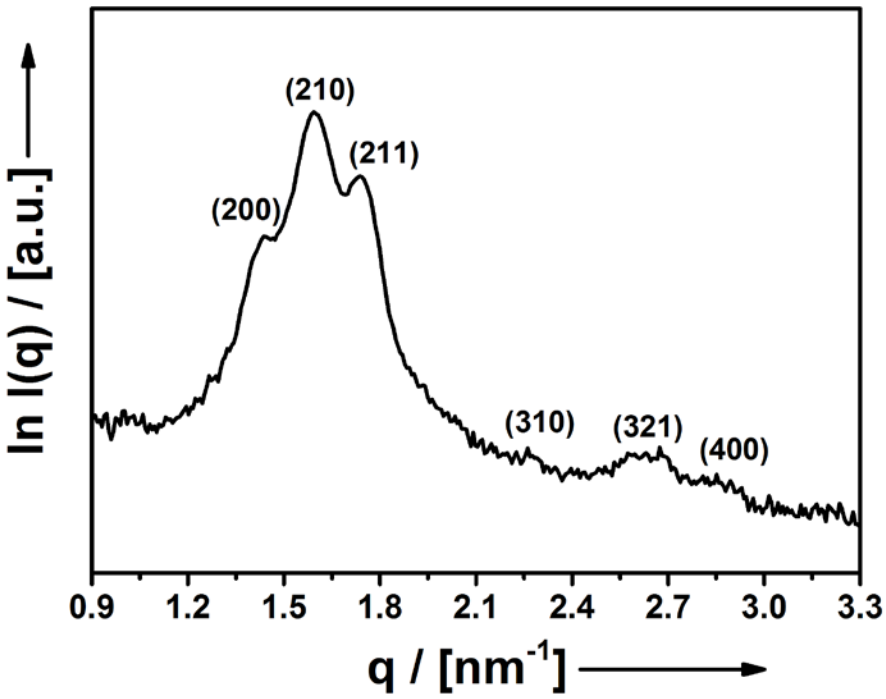

Experimental SAXS pattern and assigned diffraction signals (hkl) for cubic packing of spherical micelles (space group $P_{m\bar{3}n}$) with lattice parameter *a* = 8.74 nm).

(c) TEM analysis.

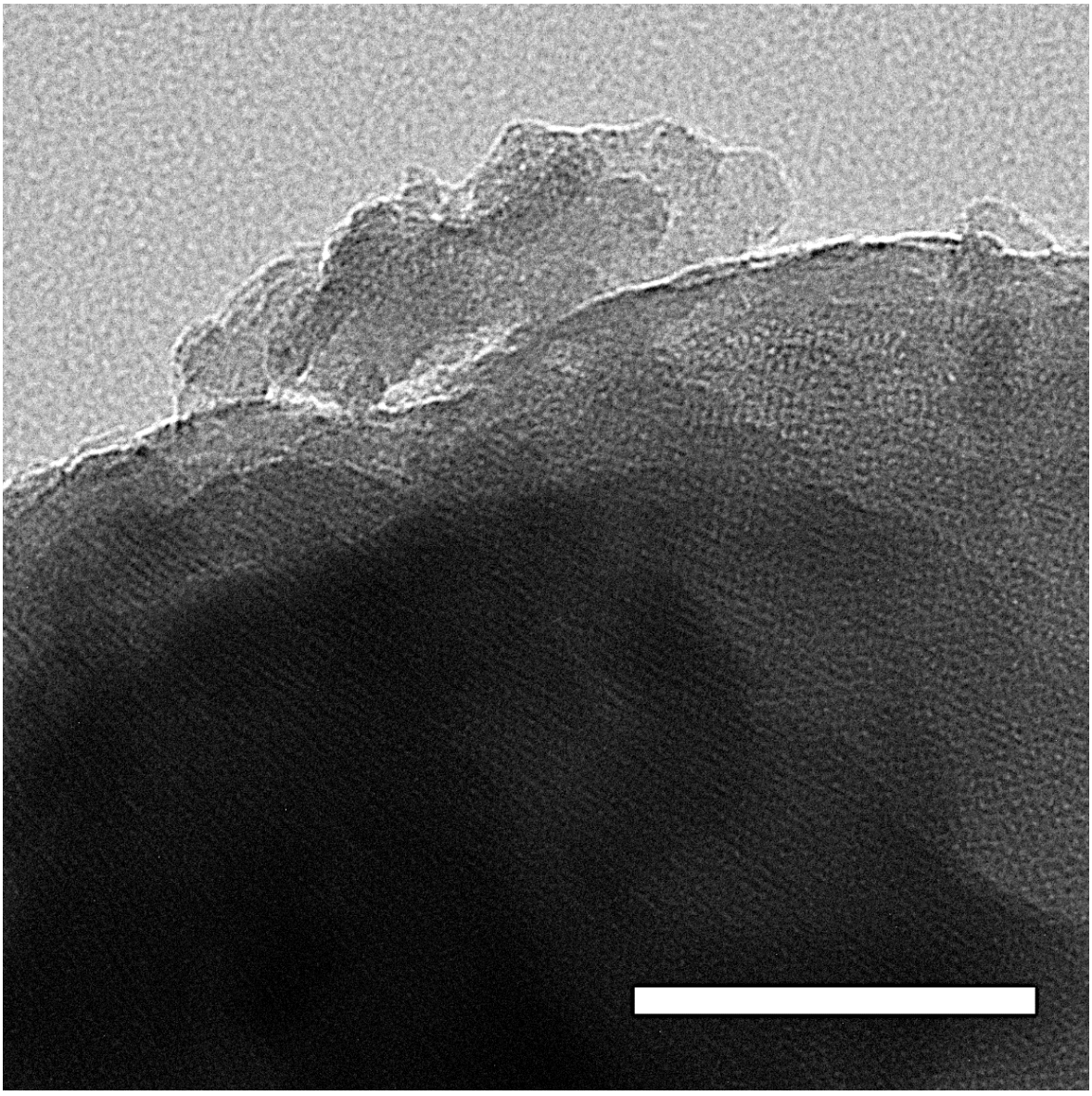

scalebar = 100 nm

(d) N_2 physisorption isotherm and pore-size distribution function.

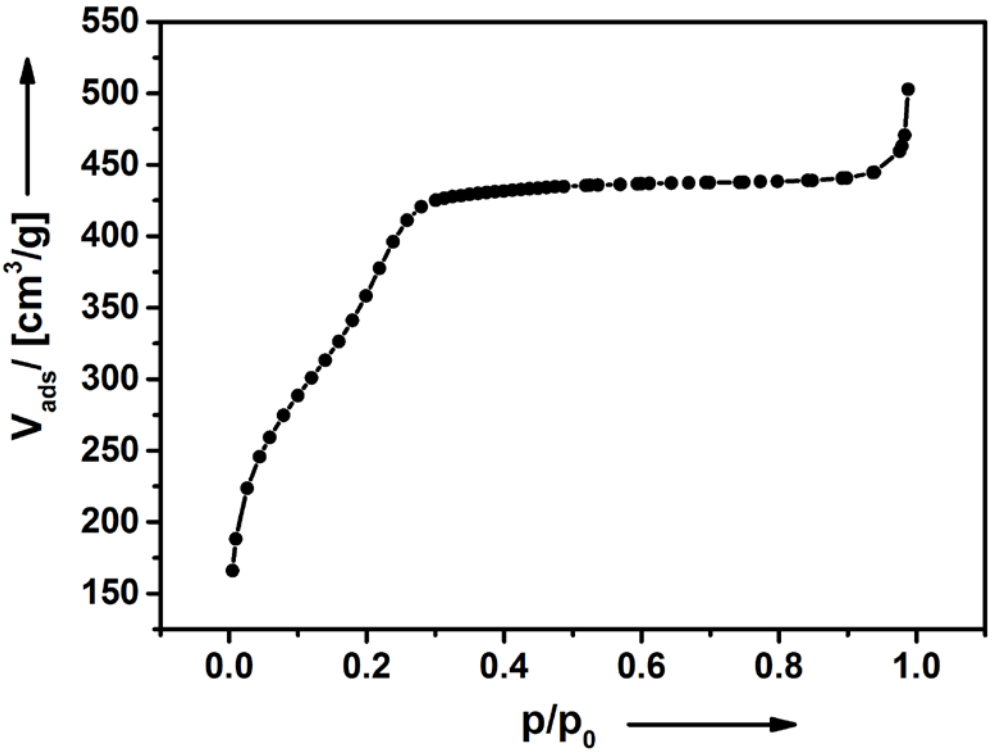

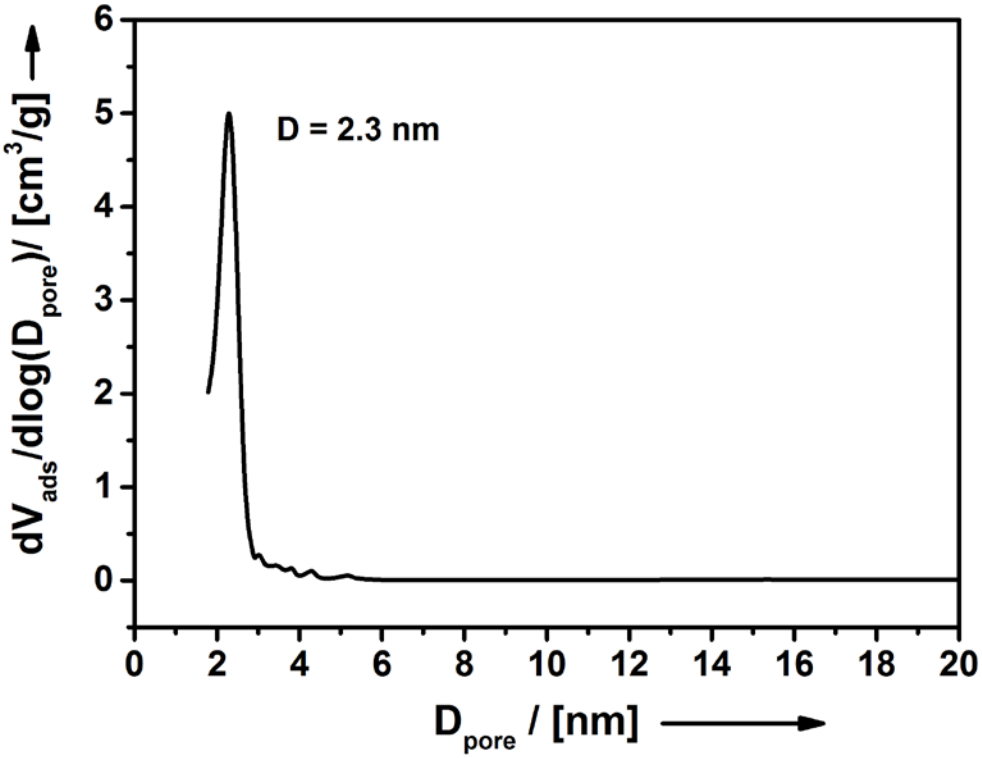

Fig. SI-9. Additional data for mesostructured silica materials obtained using MnC_{16}DOTA as a structure directing agent.

(a) SEM images of the particle shown in Fig. 4.

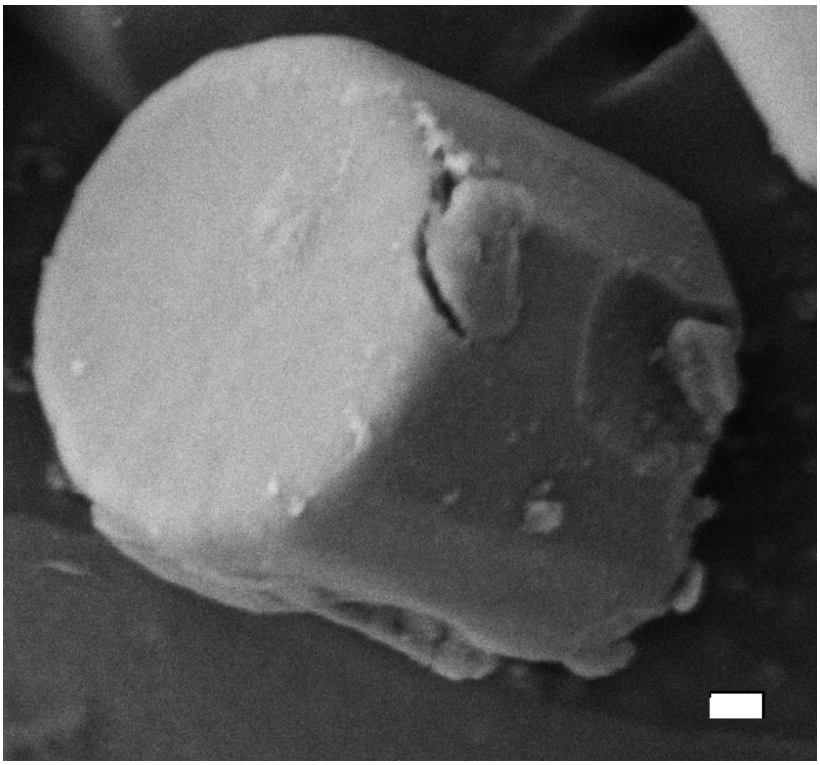

scalebar = 200 nm

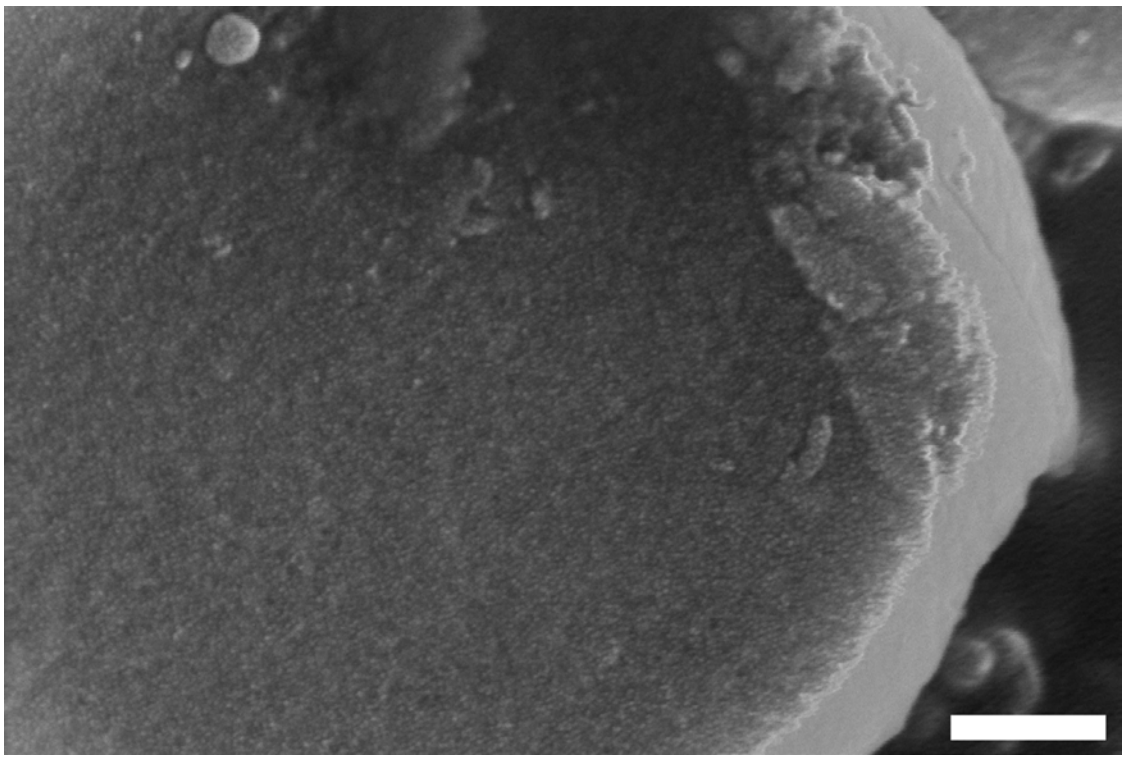

scalebar = 200 nm

(b) Alternative particles/ SEM micropgraphs

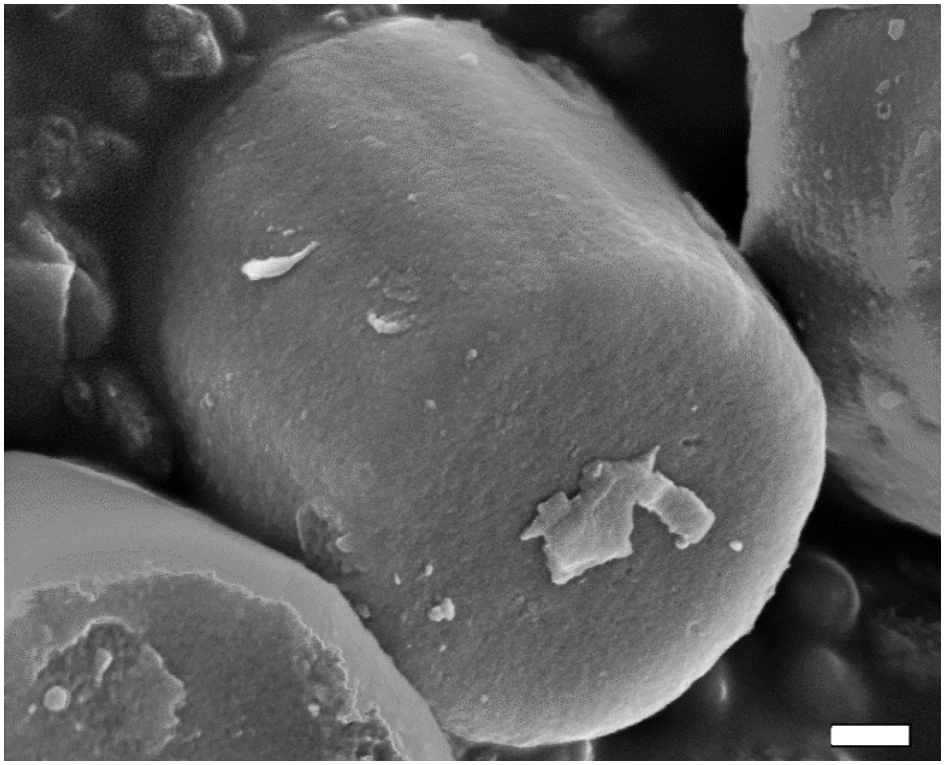

scalebar = 200 nm

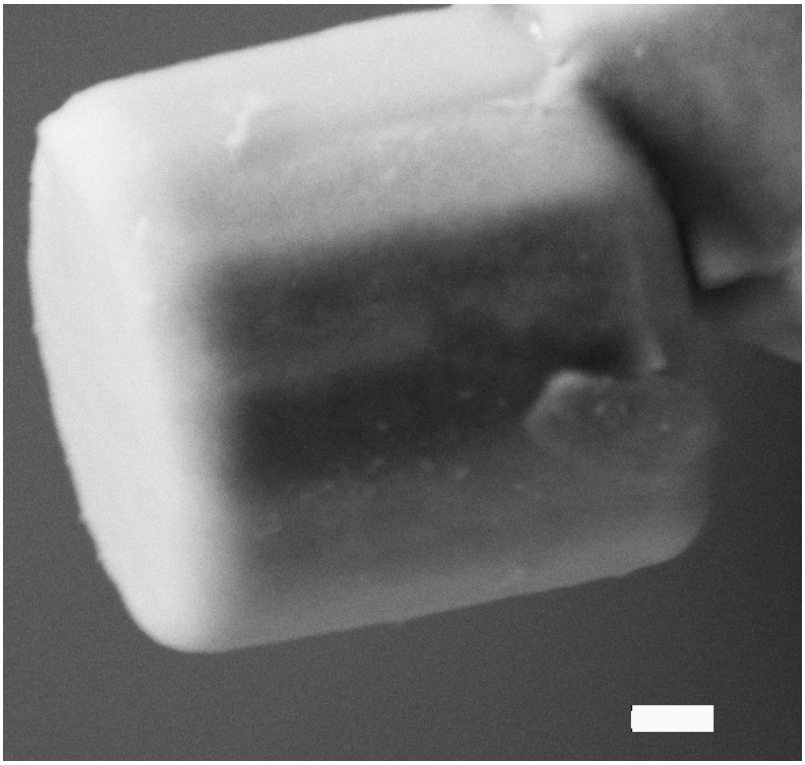

scalebar = 200 nm

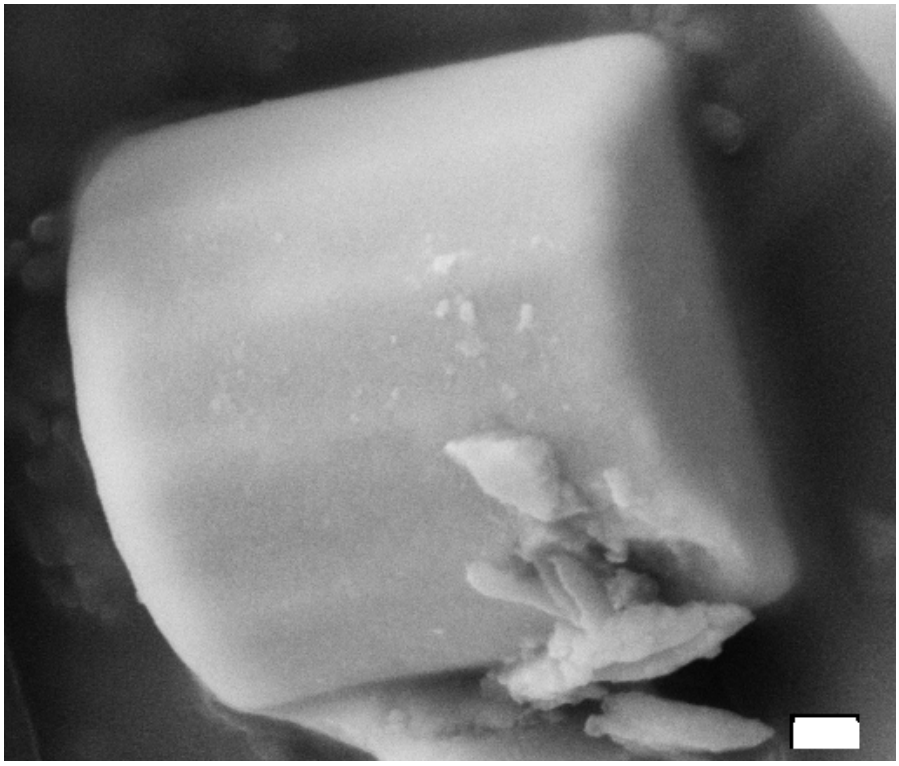

scalebar = 200 nm

(c) FIB treatment of one particle.

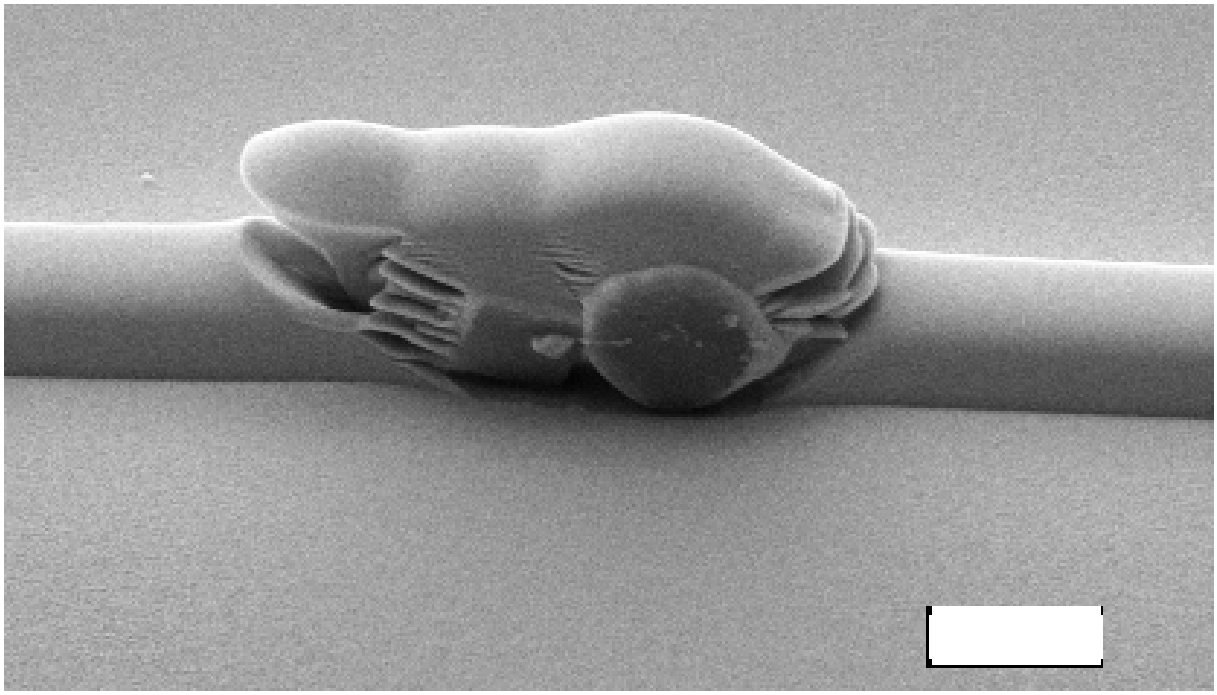

One individual mesostructured particle on silicon coated with Pt. Scalebar = 2µm.

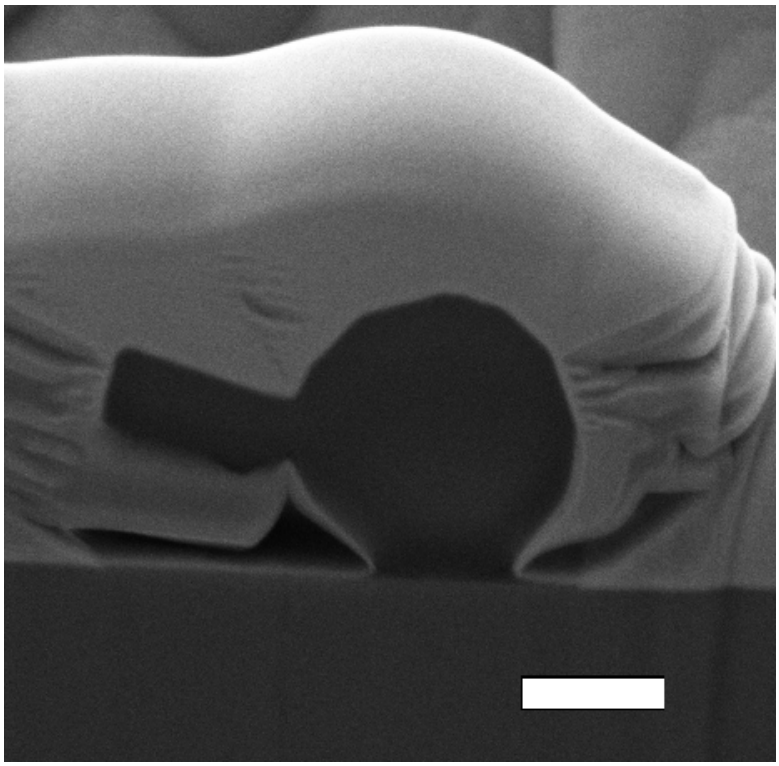

SEM analysis of the cutted slice. Scalebar = 1 µm.

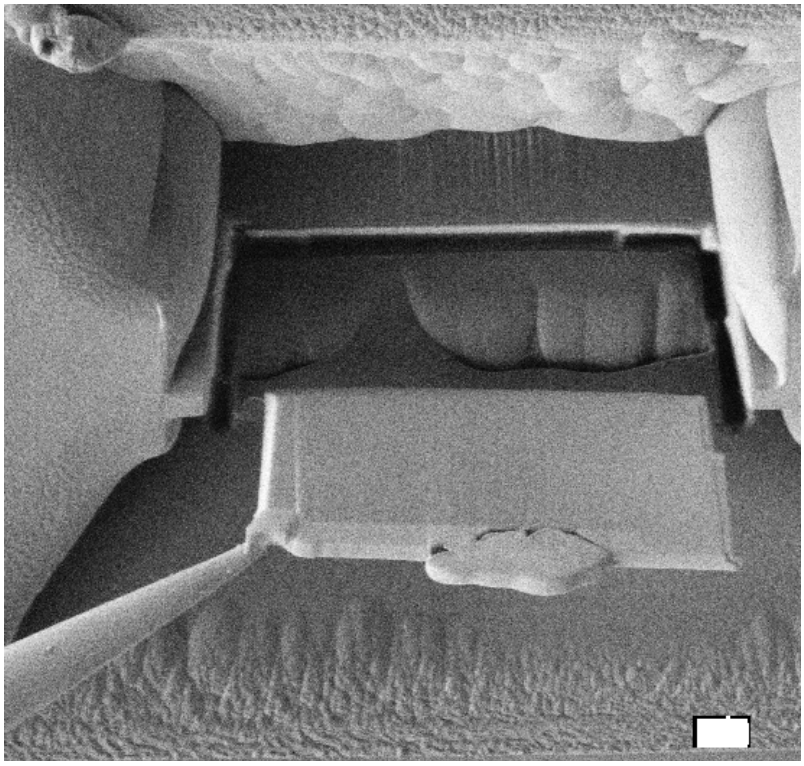

Transfer of slice to positioning needle. Scalebar = 2 μm.

(d) TEM/ EDX line scan analysis.

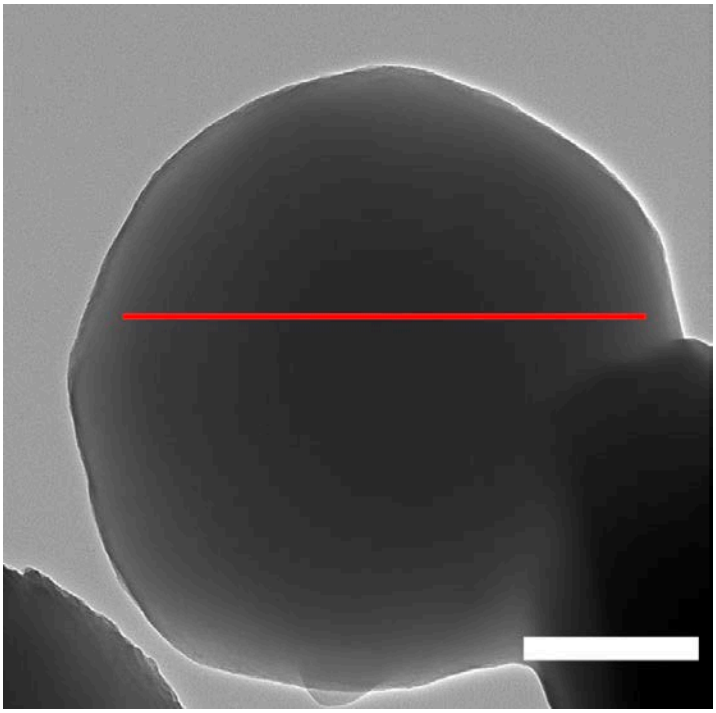

scalebar = 200 nm; red line shows the path of the EDX line scan.

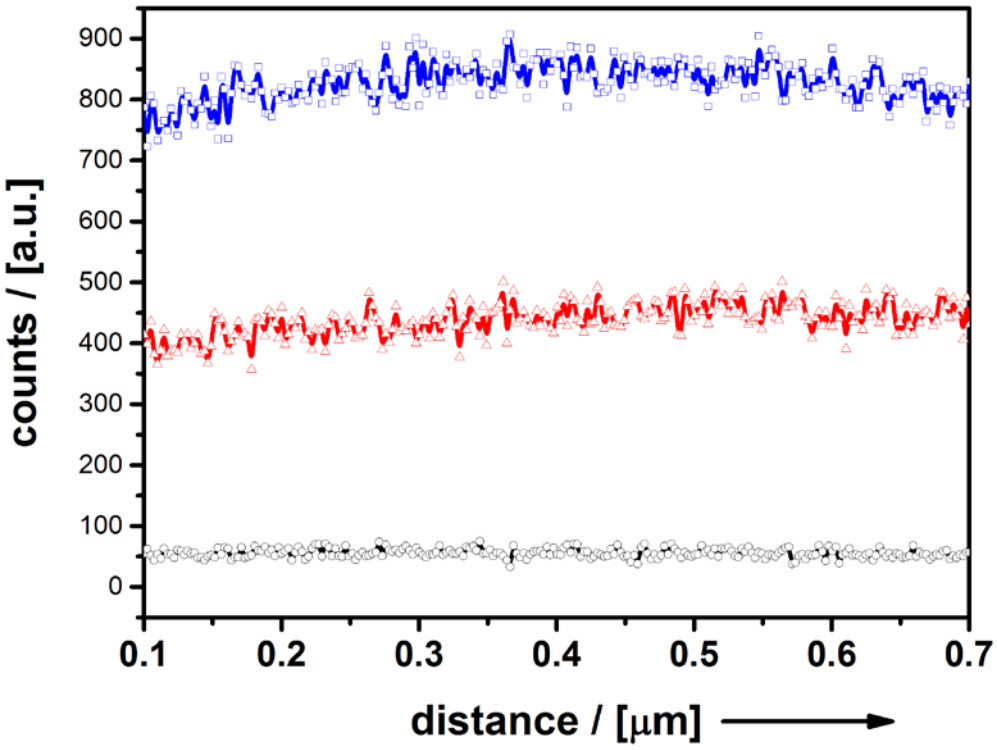

blue line ≅ EDX trace of silicon (Si); red trace ≅ EDX trace of oxygen (O); black trace ≅ EDX trace of manganese (Mn).

Mn is distributed homogeneously in the particle, as expected when the spherical micelles are composed of MnC_{16}DOTA as a surfactant.

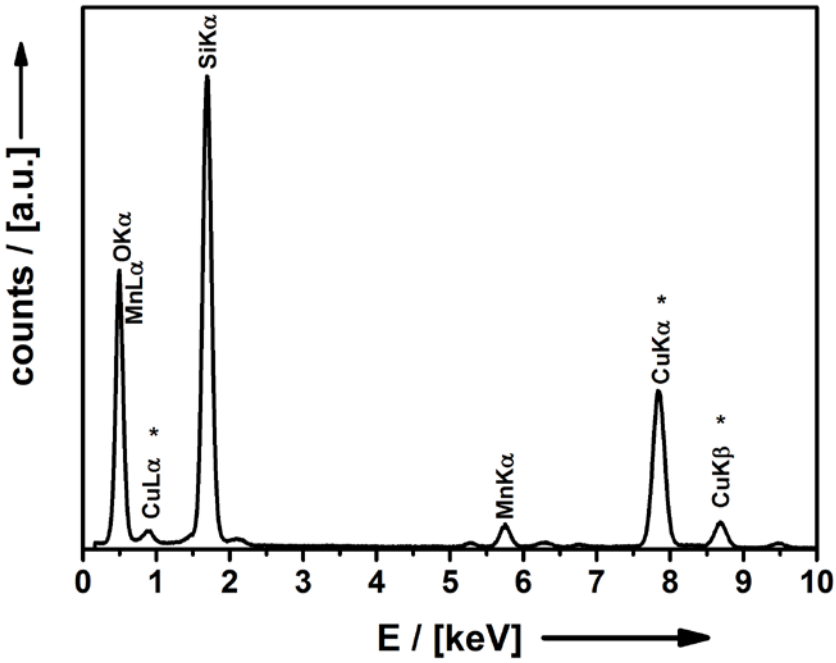

Signals for copper result from the used copper-carbon TEM grid.

(e) TEM micrograph of pore structure.

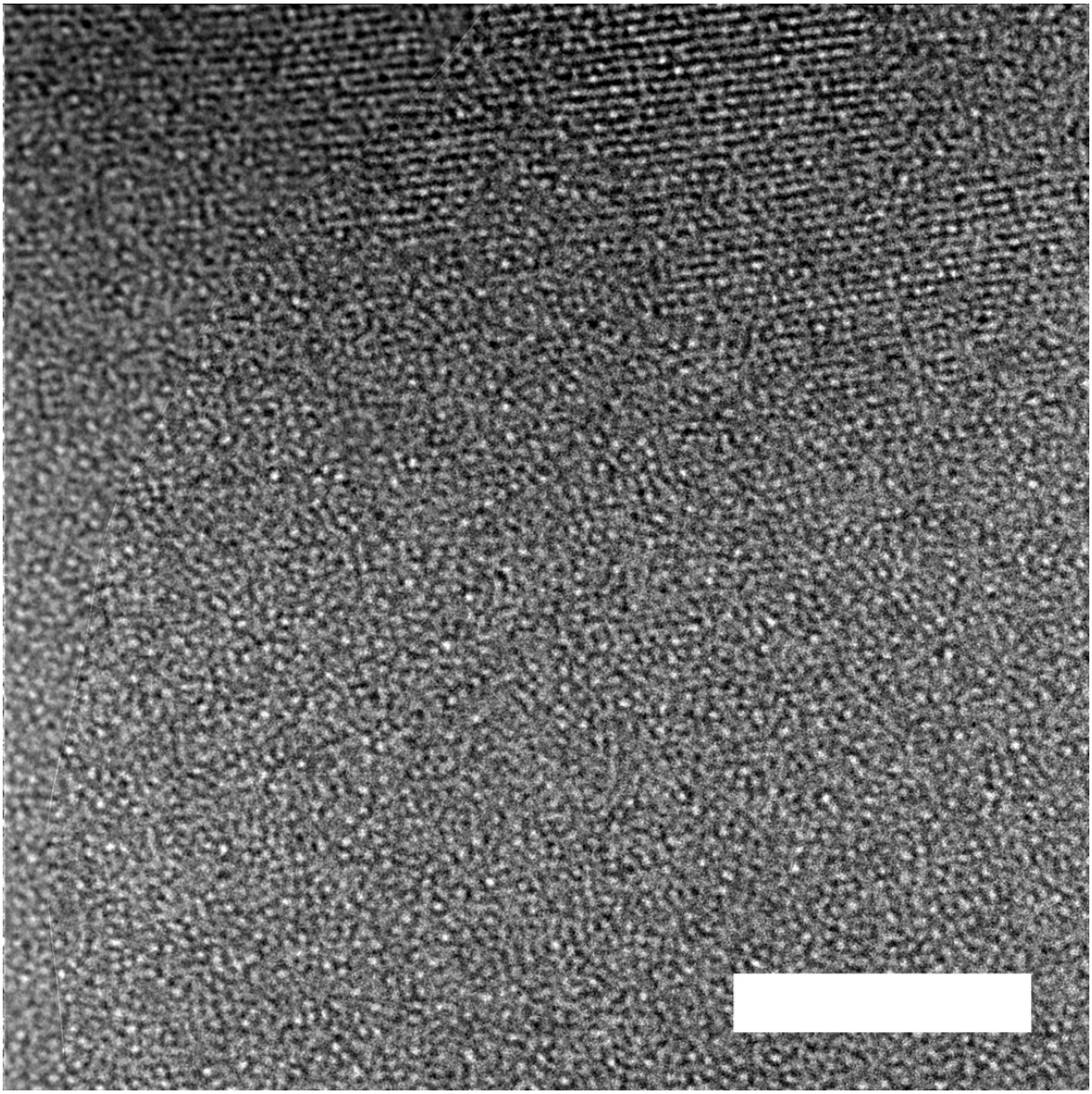

scalebar = 100 nm

(f) N_2 physisorption analysis and pore-size distribution function.

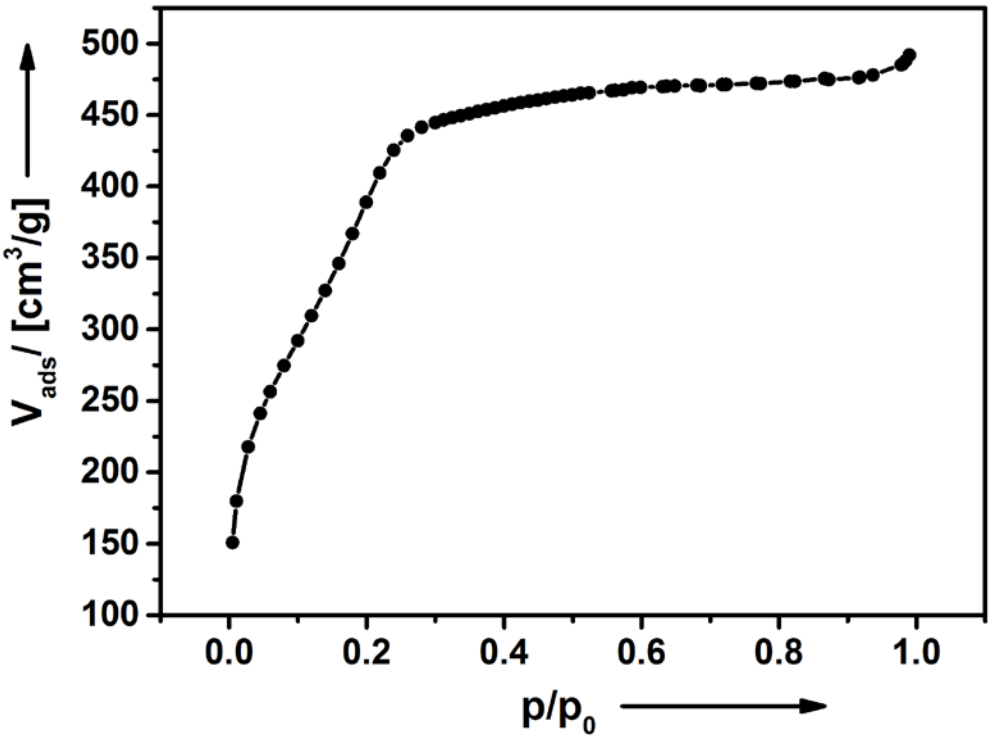

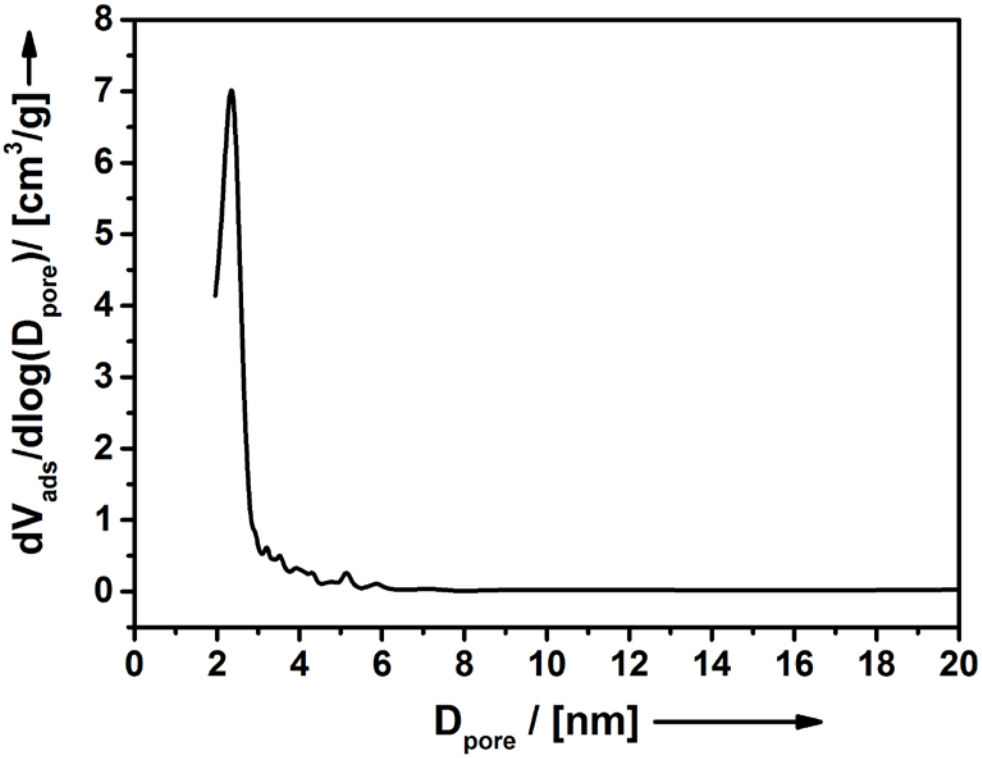

References

[1] aJ. Massue, S. E. Plush, C. S. Bonnet, D. A. Moore, T. Gunnlaugsson, *Tetrahedron Letters* **2007**, *48*, 8052-8055; bB. Jagadish, G. L. Brickert-Albrecht, G. S. Nichol, E. A. Mash, N. Raghunand, *Tetrahedron Letters* **2011**, *52*, 2058-2061; cS. Polarz, C. Bährle, S. Landsmann, A. Klaiber, *Angewandte Chemie International Edition* **2013**, *52*, 13665-13670.

[2] G. M. Sheldrick, Universität Göttingen, Göttingen, **1997**.

[3] L. J. Barbour, *Journal of Supramolecular Chemistry* **2001**, *1*, 189-191.

[4] G. Maret, G. Weill, *Biopolymers* **1983**, *22*, 2727-2744.

[5] H. B. Bürgi, *Annual Review of Physical Chemistry* **2000**, *51*, 275-296.

[6] A. Riesen, M. Zehnder, T. A. Kaden, *Helvetica Chimica Acta* **1986**, *69*, 2067-2073.

[7] aS. Amin, T. W. Kermis, R. M. van Zanten, S. J. Dees, J. H. van Zanten, *Langmuir* **2001**, *17*, 8055-8061; bG. Garg, P. A. Hassan, S. K. Kulshreshtha, *Colloid Surf. A-Physicochem. Eng. Asp.* **2006**, *275*, 161-167.